nature cell biology

A cytoplasmic dynein tail mutation impairs motor processivity

Kassandra M. Ori-McKenney[1,2,4], Jing Xu[3,4], Steven P. Gross[3,5,6] and Richard B. Vallee[1,2,5,6]

Mutations in the tail of the cytoplasmic dynein molecule have been reported to cause neurodegenerative disease in mice. The mutant mouse strain Legs at odd angles (*Loa*) has impaired retrograde axonal transport, but the molecular deficiencies in the mutant dynein molecule, and how they contribute to neurodegeneration, are unknown. To address these questions, we purified dynein from wild-type mice and the Legs at odd angles mutant mice. Using biochemical, single-molecule, and live-cell-imaging techniques, we find a marked inhibition of motor run-length *in vitro* and *in vivo*, and significantly altered motor domain coordination in the dynein from mutant mice. These results suggest a potential role for the dynein tail in motor function, and provide direct evidence for a link between single-motor processivity and disease.

Cytoplasmic dynein is a minus-end directed microtubule motor protein responsible for a variety of cellular functions, including retrograde axonal transport[1]. Two dynein mutant mouse strains, Legs at odd angles (*Loa*) and Cramping1 (*Cra1*), were identified in a screen for genes involved in late onset motor neuron disease (MND)[2]. This finding identified a new class of MND genes (including the p150Glued gene, which encodes for a subunit of dynactin, a protein of the dynein regulatory complex[3–5]; *Dctn1* in mice and *DCTN1* in humans), and significantly expanded the limited pool of familial amyotrophic lateral sclerosis (ALS) candidate genes. Of the dynein mutations, *Loa* has received particular attention[6–10]. $Loa^{+/-}$ mice were initially reported to exhibit lower motor neuron degeneration, but recent studies have found severe loss of sensory neurons[8,9]. *Loa* mutant mice also exhibited a decreased rate of retrograde axonal transport[2,10]. The *Loa* mutation (F580Y) resides in the amino-terminal region of the dynein heavy chain polypeptide, within the dynein 'tail'. This region is responsible for organizing the multiple dynein subunits into a complex and for binding to membranous cargo. Dynein generates force through its two motor domains, each located at the carboxy-terminal end of the heavy chain, 1,500 amino acids (15–20 nm) from the site of the *Loa* mutation. Whether and how the *Loa* mutation affects cytoplasmic dynein function has remained untested.

To approach this problem, we first tested the ability of dynein to remain associated with membranous vesicles isolated by sucrose step gradient flotation from the brains of wild-type, $Loa^{+/-}$ and $Loa^{-/-}$ mice. No clear difference could be detected (Fig. 1a). The *Loa* mutation lies in the region of the dynein heavy chain involved in heavy chain–heavy chain dimerization and in heavy chain–intermediate chain binding (Supplementary Information, Fig. S1). We therefore tested for potential defects in the stability of the mutant complex. Fractionation of whole brain cytosol by sucrose density gradient centrifugation revealed a single major 20S dynein peak for both the wild-type and $Loa^{+/-}$ mutant animals. In contrast, dynein from $Loa^{-/-}$ mice demonstrated a small, but reproducible, decrease in dynein S value, accompanied by the appearance of a free intermediate-chain peak (12 ± 2% of total intermediate chains) at 6S (Supplementary Information, Fig. S2a). To test whether these observations reflect a more general reduction in mutant dynein stability, we exposed brain extracts to potassium iodide (KI), a chaotropic salt to which dynein is particularly sensitive[11]. In the presence of KI, dynein dissociation increased both as a function of KI concentration and the proportion of mutant dynein heavy chain (Supplementary Information, Fig. S2b–d). These results indicate that the *Loa* mutation may impair the interactions between subunits.

To gain further insight into the molecular effects of the *Loa* mutation, we purified cytoplasmic dynein from wild-type and $Loa^{+/-}$ adult mouse brains[1]. As observed in brain cytosol, the purified mutant dynein remained intact by sucrose density gradient centrifugation (data not shown). The dynein purified from $Loa^{+/-}$ mice had no differences in subunit composition when compared with the wild-type mouse protein, and neither preparation had detectable levels of the processivity factor dynactin, as assessed by Coomassie-blue staining and immunoblotting (Fig. 1b and Supplementary Information, Fig. S3a, b). As mice homozygous for the *Loa* mutation die shortly after birth, the amounts of brain tissue we could obtain were inadequate to purify biochemical amounts of dynein by this procedure. Nonetheless, we were able to purify small amounts of dynein from $Loa^{-/-}$ mice for single molecule analysis using a modification of this method (Figs 2 and 3 and Supplementary Information, Fig. S3c, d).

[1]Department of Pathology and Cell Biology, Columbia University. New York, NY 10032, USA. [2]Department of Biological Sciences, Columbia University, New York, NY 10027, USA. [3]Department of Developmental and Cell Biology, University of California, Irvine, CA 92697, USA. [4]These authors contributed equally to this work. [5]Co-senior authors. [6]Correspondence should be addressed to R.B.V. or S.P.G. (e-mail: rv2025@columbia.edu or sgross@uci.edu)

Received 14 July 2010; accepted 14 October 2010; published online 21 November 2010; DOI: 10.1038/ncb2127

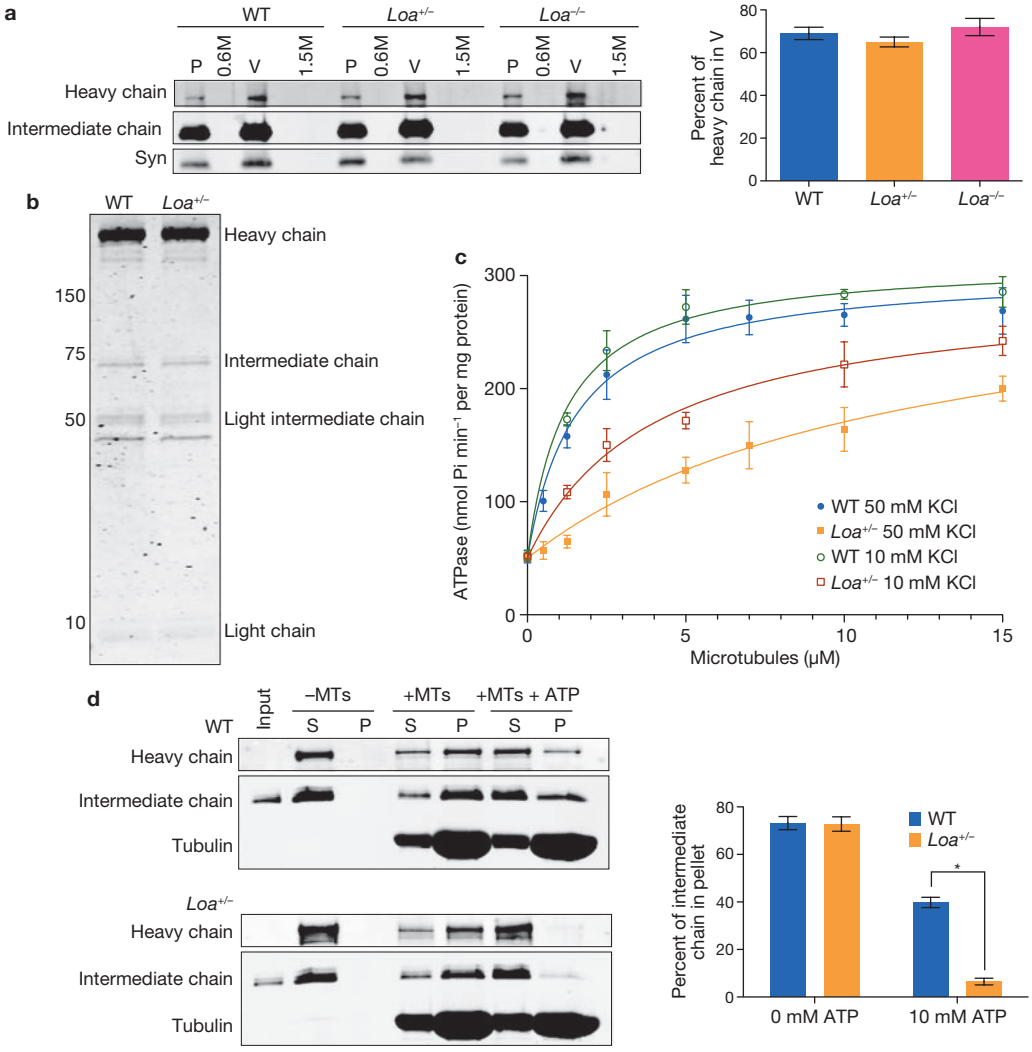

Figure 1 Purification and biochemical analysis of wild-type and mutant cytoplasmic dynein. (**a**) Pellets containing vesicles isolated from the brains of the indicated mice strains were fractionated by flotation through a 2M, 1.5M and 0.6M sucrose step gradient. Vesicles floated to the 0.6–1.5 M interface. Left: immunoblot of samples taken from the pellet (P), 0.6 M sucrose step (0.6), vesicles at the sucrose interface (V) and the 1.5 M sucrose step (1.5 M), using antibodies against the heavy and intermediate chains of dynein (synaptotagmin was used as a marker for vesicles). Right: percentage of heavy chain in vesicles was quantified from band intensities in the immunoblot (n = 3 experiments, data are means ± s.d.). WT; wild-type mice. (**b**) Coomassie-stained gel of cytoplasmic dynein purified from the brains of wild-type and *Loa*$^{+/-}$ mice. (**c**) ATPase activity of dynein purified from wild-type and *Loa*$^{+/-}$ mice as a function of microtubule concentration, at low- and high-ionic strength. Activity data are means ± s.d., determined from $n = 3$ experiments (10 mM KCl), or from $n = 6$ experiments (50 mM KCl) and fitted with Michaelis-Menten kinetics. **(d)** Left: dynein purified from wild-type (top) or *Loa*$^{+/-}$ (bottom) mice were incubated with microtubules (MTs) and ATP, as indicated. After centrifugation, binding of dynein was assessed by immunoblotting for heavy chain, intermediate chain and tubulin in the supernatant (S) or microtubule-containing pellet (P) fractions. Input is 20% of total protein. Right: amount of dynein in the microtubule pellet in the absence and presence of ATP. Data are means ± s.d. from $n = 3$ different experiments per genotype, per ATP condition (Asterisk indicates $P < 0.001$). Uncropped images of blots are shown in Supplementary Information, Fig. S1.

To test the effects of the *Loa* mutation on dynein mechanochemical activity, we measured the ATPase activity of dynein purified from wild-type and *Loa*$^{+/-}$ mice in the presence and absence of microtubules. The basal ATPase activity was similar for dynein from both wild-type and *Loa*$^{+/-}$ mice: 51.3 ± 5.3 and 51.7 ± 3.3 nmol Pi min^{-1} per mg of dynein, respectively (Fig. 1c). However, in the presence of microtubules, the ATPase activities of wild-type and mutant dynein differed markedly. The Michaelis constant for microtubules, K_{mMT}, was 1.5 ± 0.2 μM for the purified wild-type dynein, similar to the value for bovine cytoplasmic dynein[12], whereas the K_{mMT} for dynein from *Loa*$^{+/-}$ mice was significantly higher, 11.8 ± 3.4 μM ($P < 0.001$). In contrast, the maximum rate (V_{max}) values were similar (wild-type = 255 ± 9 nmol min^{-1} per mg; *Loa*$^{+/-}$ = 263 ± 43 nmol min^{-1} per mg). The latter results indicate that the maximal ATP turnover rate is unaffected by the *Loa* mutation. However, the increased K_{mMT} suggests a marked decrease in the effective affinity of the mutant dynein for microtubules during ATP hydrolysis. In support of this, the K_{mMT} for dynein from *Loa*$^{+/-}$ mice was partially rescued at reduced ionic strength (4.0 ± 0.6 μM, compared with 1.2 ± 0.2 μM for wild-type), which increases the affinity of dynein for microtubules[12]. Furthermore, microtubule binding by the purified mutant dynein was markedly reduced, compared with wild-type dynein, in the presence of ATP, but not in its absence (apo state; Fig. 1d). From this surprising result,

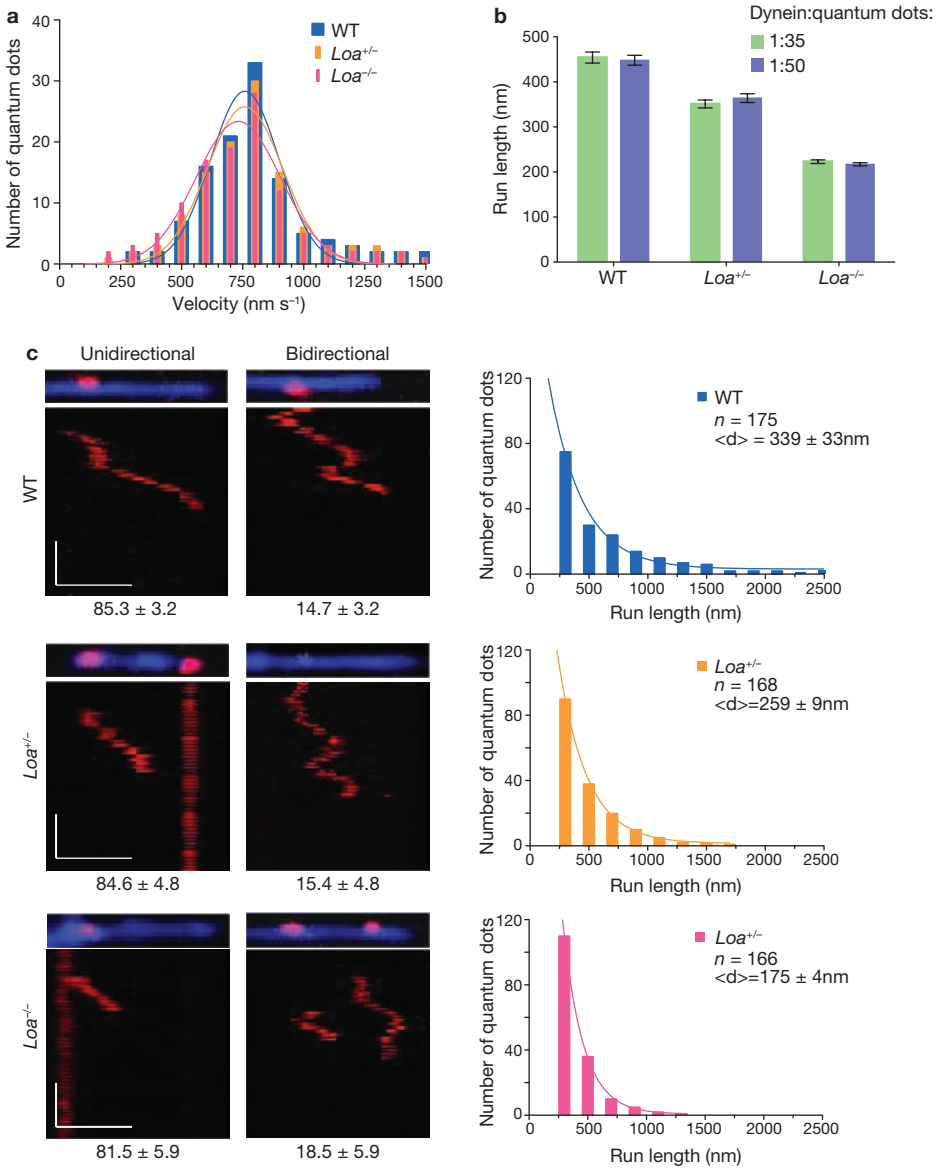

Figure 2 Single-molecule dynamics of cytoplasmic dynein isolated from wild-type and mutant mice. Dynein was linked to quantum dots using an antibody to the intermediate chain, and then applied to microtubules in the absence of ATP, and monitored by fluorescence microscopy in the presence of 500 μM ATP. (**a**) Velocities for quantum dot runs > 200 nm for dynein isolated from wild-type, *Loa*$^{+/-}$, and *Loa*$^{-/-}$ mice ($n > 111$ quantum dots). (**b**) Average run-length at molar ratios of dynein:quantum dots of 1:35 and 1:50. Data are means ± s.e.m, $P < 0.001$ for dynein isolated from mutant mice, compared with wild-type mice ($n = 175$, 168 and 166 for wild-type, *Loa*$^{+/-}$ and *Loa*$^{-/-}$ mice, respectively). (**c**) Left: representative kymographs of dynein-bound quantum dots on microtubules. Top images show initial position of dynein-bound quantum dot on a microtubule (purple). The percentage of quantum dots that exhibited unidirectional and bidirectional dynamics is indicated below the kymographs ($n = 175$, 168 and 166 for wild-type, *Loa*$^{+/-}$ and *Loa*$^{-/-}$ mice, respectively). Scale bars, 1 μm (*x* axis) and 5 s (*y* axis). Right: distribution of net run lengths. *n* values and mean square displacement (± s.e.m.) are indicated.

it seems that much of the dynein fraction normally seen to co-sediment with microtubules in the presence of ATP is engaged in active, processive movement along the microtubule. These results suggest that the *Loa* mutation affects the interaction of dynein with microtubules during the ATPase and force-generating portion of the crossbridge cycle, but not in the strong microtubule-binding (apo) state.

To gain insight into the underlying molecular defects of dynein from *Loa* mutants, we used quantum-dot and optical-trap assays under single-molecule conditions. Wild-type and mutant dynein were attached to quantum dots using antibodies specific to the dynein tail, and the velocity and run-length of these particles was then analysed. Movements in the two dynein preparations were ATP-dependent and at a velocity similar to that reported for mouse dynein–dynactin complexes (Fig. 2a and Supplementary Information, Fig. S4a)[13]. The purified wild-type and mutant dyneins had predominantly unidirectional movements, but some bidirectional events were also observed, as previously reported (Fig. 2c)[13–15]. However, a clear difference was observed in the wild-type versus mutant dynein run-lengths (Fig. 2b, c). Wild-type dynein had an average run-length of 339 ± 33 nm (Fig. 2c), about half that of mouse dynein–dynactin complexes[13] (consistent with the absence of dynactin in our

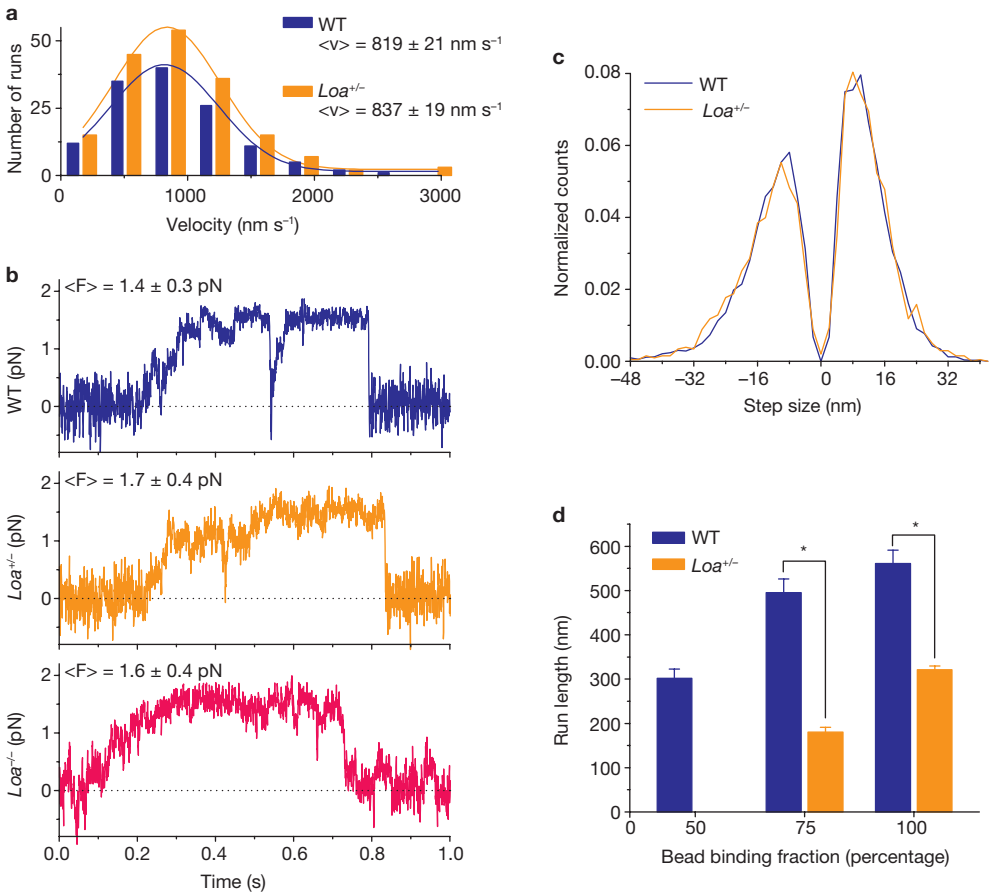

Figure 3 Optical-trap analysis of wild-type and mutant cytoplasmic dynein dynamics in single- and multi-motor regions. The fraction of beads bound to microtubules was used as an indicator for the average number of available motors per bead: ≤ 30% corresponds to single-motor levels and > 50% to multiple-motor levels (Supplementary Information). Dynein-coated beads were positioned on a microtubule using an optical trap. (**a**) Distribution of run velocities for beads attached to dynein isolated from wild-type or *Loa*$^{+/-}$ mice. The mean velocity ± s.e.m. is indicated for dynein isolated from each mouse strain (n = 110 and 135 runs for dynein isolated from wild-type and *Loa*$^{+/-}$ mice, respectively; P = 0.97). (**b**) Representative single-motor stall force traces for dynein purified from mice with the indicated genotypes. After positioning of the dynein-bound beads on a microtubule, a trap stiffness of 2.2 pN per 100 nm was applied. A stall was scored if the bead proceeded away from the trap centre and held its plateau position for > 200 ms before detachment. The mean stalling force ± s.d. is indicated for dynein isolated from each mouse strain (n = 29, 34 and 51 stalls for wild type, *Loa*$^{+/-}$ and *Loa*$^{-/-}$ dynein, respectively). The standard deviations from the mean for the stall forces are consistent with the systematic noise of the optical trap, 0.3–0.4 pN. (**c**) Distribution of axial step sizes for beads bound to dynein, purified from wild-type and *Loa*$^{+/-}$ mice, under 2.2 pN per 100 nm applied load (n = 7269 and 1979 axial steps for wild-type and *Loa*$^{+/-}$ dynein, respectively, P = 0.89). The two peaks represent both forward and backward stepping for dynein isolated from wild-type and *Loa*$^{+/-}$ mice. The bulk of steps larger than 8 nm in both directions represent unresolved, consecutive 8 nm steps (see Supplemental Information). (**d**) Run-lengths of beads were measured at the indicated bead–microtubule binding fractions. Data are means ± s.e.m. Wild-type: n = 38, 64 and 127 runs for binding fraction of 50, 75, and 100%, respectively; *Loa*$^{+/-}$: n = 39 and 296 runs for binding fraction of 75 and 100%, respectively. Asterisks indicate $P < 0.03$). *Loa*$^{+/-}$ run-length at 50% binding fraction was below measurement limit under assay conditions used here (Supplementary Information, Fig. S4c).

dynein preparations). Dynein from *Loa*$^{+/-}$ mice had fewer long runs and a 23% shorter average run-length (259 ± 9 nm). Dynein from *Loa*$^{-/-}$ mice was even more impaired, with an average run-length approximately half that of wild-type dynein (175 ± 4 nm; Fig. 2c). Optical-trap experiments using the same dynein preparations adsorbed to polystyrene beads gave comparable results. There was no difference in the average velocity, but there was a similar reduction in the single-motor processivity, of dynein from *Loa*$^{+/-}$ mice, compared with dynein from wild-type mice (Fig. 3a and Supplementary Information, Fig. S4b, c). Based on the motility data, we calculate a 31% and 37% increase in the average off-rate, at 0.5 mM and 1 mM ATP, respectively, for dynein from *Loa*$^{+/-}$ mice, compared with wild-type dynein (Supplementary Information). This is consistent with the enhanced dissociation of *Loa*$^{+/-}$-mouse dynein from microtubules in the presence of ATP (Fig. 1). Consistent with results for bovine cytoplasmic dynein, the stall force for single wild-type-mouse dynein molecules was 1.4 ± 0.3 pN, and within experimental error of the forces measured for dynein from *Loa*$^{+/-}$ mice (1.7 ± 0.4 pN) and *Loa*$^{-/-}$ mice (1.6 ± 0.4 pN; Fig. 3b)[14,16]. We also observed no difference in the step size of the wild-type or mutant dynein motors while they moved along microtubules under load (Fig. 3c and Supplementary Information, Fig. S5a–c).

Physiological cargoes typically use multiple motors. To assess how the observed defects in dynein processivity translate to the *in vivo* condition, we measured the run-lengths of wild-type and *Loa* mutant dyneins *in vitro* and found an increase in run-length for multi-motor conditions (as previously reported in ref. 17). However, this increase was attenuated for dynein from *Loa*$^{+/-}$ mice (Fig. 3d). Computational modelling of

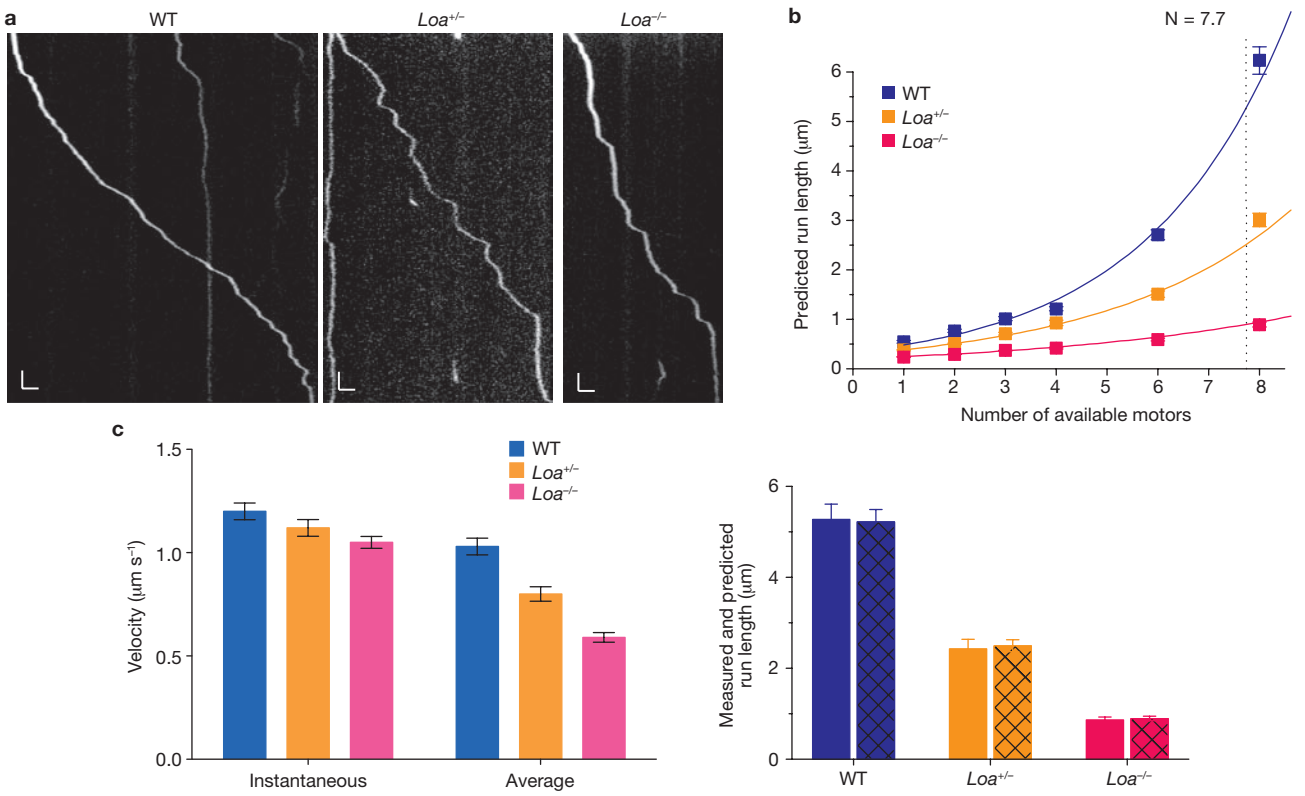

Figure 4 Analysis of retrograde transport of lysosomes in wild-type and mutant axons, with theoretical comparison. (**a**) Kymographs of retrograde lysosome transport in axons isolated from mice with the indicated genotype. Images used to generate kymographs were representative of processive lysosome runs. Scale bars, 5 mm (*x* axis) and 5 s (*y* axis). (**b**) Top: simulations of how motor number affects run length. The simulation was constrained by the experimental measurements of single-motor processivity from this study. Simulated data was used to predict number of motors (N; indicated by dotted line) involved in axonal transport of lysosomes, based on *in vivo* measurements of run-length in wild-type mice (5.27 ± 0.34 μm). Bottom: comparison of *in vivo* measurements of lysosome run-length (solid bars) and run-lengths calculated from simulations (hatched bars), using an average of 7.7 dynein motors per cargo as calculated from simulation shown at the top. Data are means ± s.e.m., $n > 400$, 300 and 600 simulated runs for wild type, $Loa^{+/-}$ and $Loa^{-/-}$, respectively and $n = 68$, 78 and 55 uninterrupted retrograde runs in neurons isolated from wild type, $Loa^{+/-}$ and $Loa^{-/-}$ mice, respectively. (**c**) Instantaneous and average lysosome velocities ± s.e.m. for each genotype ($n = 102$, 98 and 111 analysed lysosomes from wild type, $Loa^{+/-}$ and $Loa^{-/-}$ mice, respectively. $P < 0.001$ for lysosome average velocity in axons from mutant mice, compared with wild-type mouse neurons).

dynein run-lengths at more extensive motor:cargo ratios demonstrated that the mean travel defect persisted with up to three or more dynein molecules per cargo, with and without adding the potential effects of *in vivo* factors into the simulation, such as the presence of dynactin[13,18,19] (Fig. 4b, top and Supplementary Information, Fig. S6a, b). An additional consequence of decreased single-molecule processivity is a reduction in the number of instantaneously engaged motors per cargo in the multiple motor range, which in turn further limits cargo travel (Supplementary Information, Fig. S6b). These simulations reveal a previously unappreciated sensitivity of multiple-motor run-lengths to changes in single-motor processivity, which is especially apparent here where the single-motor processivity is low, compared with bovine dynein.

The *Loa* mutation has been linked to defects in retrograde axonal transport[2]. To compare the effects of the *Loa* mutation *in vivo* with our *in vitro* data, we performed live-cell imaging analysis of lysosome/late endosome dynamics at high temporal resolution (5 frames s^{-1}; Fig. 4a–c). Custom analysis software was then used to precisely identify periods of uninterrupted motion ('runs', for definition see Supplemental Information) towards the cell body. The far distal region of the axon was imaged (> 100 μm from cell body) and predominantly unidirectional, retrograde runs were observed, as previously described[20]. Retrograde run-lengths were reduced by 53% and 83% in neurons from $Loa^{+/-}$ and $Loa^{-/-}$ mice, respectively ($P < 0.001$, Fig. 4b, bottom and Supplementary Information, Fig. S6c). The wild-type *in vivo* run-length (5.27 ± 0.34 μm) allowed us to use the simulated data shown in Figure 4b to estimate an average of 7.7 dynein molecules per cargo, similar to recent values based on stall force and biochemical isolation[21,22]. We then predicted the expected mutant run-lengths with 7.7 dyneins per cargo, adjusting only the single-motor processivity to reflect the measured *in vitro* processivity defects. The predicted run-lengths were in excellent agreement with those measured *in vivo* (2.49 ± 0.13 versus 2.43 ± 0.21 μm for dynein from $Loa^{+/-}$ mice; 0.89 ± 0.05 versus 0.86 ± 0.07 μm for $Loa^{-/-}$ mice; Fig. 4b, bottom). No difference was found in the instantaneous velocity of lysosomes when comparing wild-type with *Loa* mutant neurons (Fig. 4c, left), which is consistent with the *in vitro* experiments (Figs 2a and 3a). However, the average velocity was reduced by 22% in $Loa^{+/-}$ and 43% in $Loa^{-/-}$ neurons when compared with wild-type (Fig. 4c, right), consistent with an increase in run terminations, and comparable to theoretical prediction (11% decrease in average velocity for dynein from $Loa^{+/-}$ mice and 37% for dynein from $Loa^{-/-}$ mice; Supplementary Information). These results suggest that the *Loa* dynein processivity defect identified *in vitro* can account for the observed impairment in retrograde axonal transport.

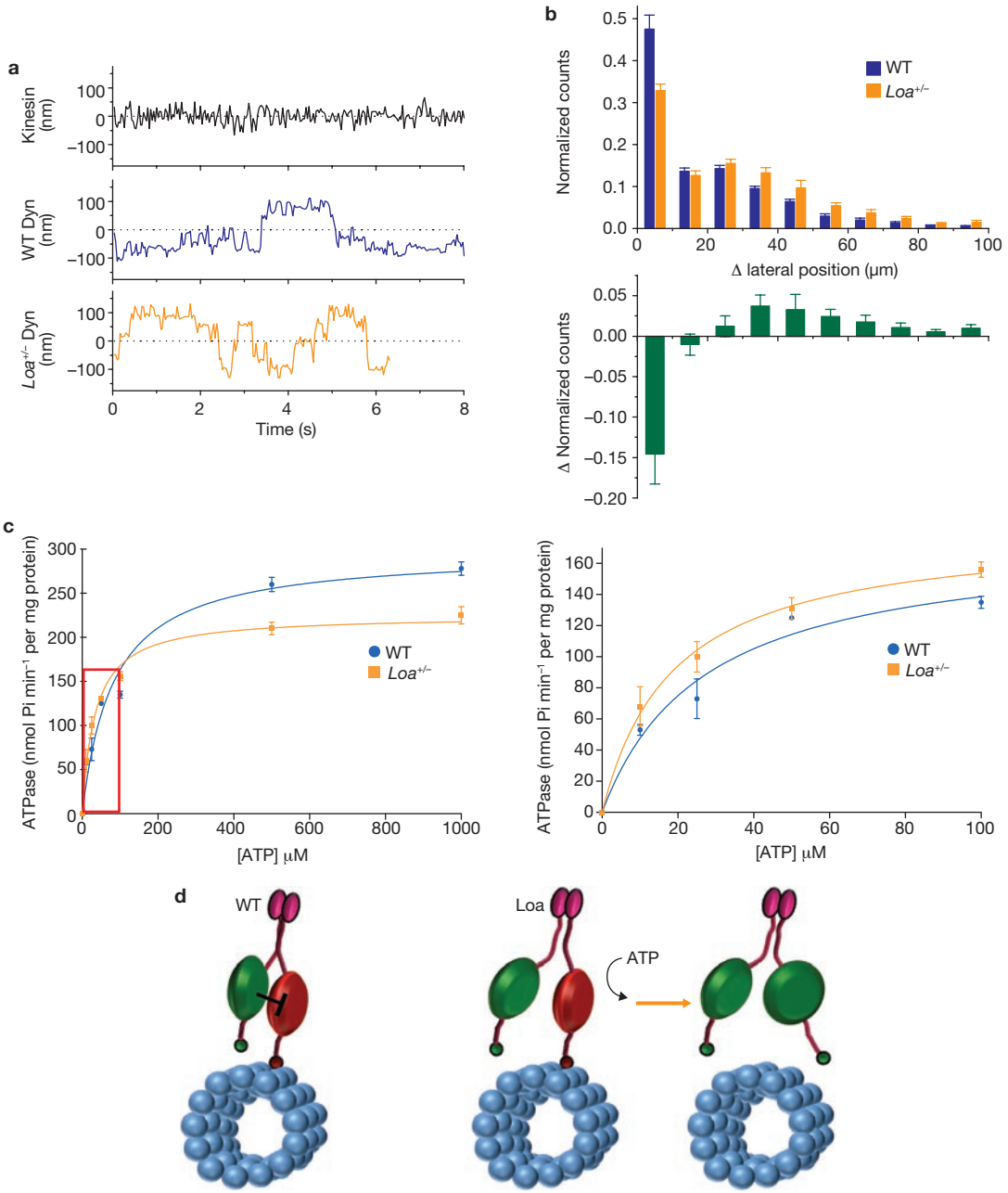

Figure 5 Biophysical and biochemical evidence of altered motor coordination in mutant dynein. (**a**) Representative lateral-position traces of beads carried by a single kinesin, or a dynein isolated from wild-type or *Loa*$^{+/-}$ mouse. (**b**) Top: distribution of the changes in lateral position of beads attached to dynein purified from wild-type and *Loa*$^{+/-}$ mice. Bottom: difference in counts shown at the top demonstrates a significant deviation of mutant dynein from wild-type ($n = 32$ and 18 runs for wild-type and *Loa*$^{+/-}$ dynein, respectively; $P < 0.05$). Error bars represent s.d. (**c**) Effect of ATP concentration on the ATPase activity of dynein purified from wild-type and *Loa*$^{+/-}$ mice, incubated with 10 μM microtubules. Low ATP concentration range indicated in graph on left is expanded in graph on the right. Activities ± s.d. were determined from three different experiments per genotype and fitted with Michaelis-Menten kinetics. (**d**) Proposed effect of *Loa* mutation on motor coordination. In wild-type dynein, the stepping head (green) inhibits the tightly bound head (red) from binding ATP. In *Loa* dynein, the stepping head (green) does not adequately inhibit the tightly bound head (red), which binds ATP prematurely and causes release from the microtubule.

To gain further insight into the mechanism responsible for altered *Loa* dynein processivity, we tested for the reported tendency of cytoplasmic dynein to step laterally on the microtubule surface, in contrast to the strict linear travel of kinesin[15,23]. Lateral stepping was confirmed in mouse dynein, and furthermore, there was a significant increase in its frequency for the mutant protein from *Loa*$^{+/-}$ mice (Fig. 5a, b). One potential explanation for this result is a disrupted coordination between the two motor domains within the native dynein complex. A gating mechanism between dimeric motor domains is well established for kinesins and myosins, but is not well understood for dynein[24–26]. Gating contributes to processive motion by ensuring that, as one motor domain advances, the other remains strongly associated with its track in the apo state, thereby preventing premature detachment[26]. As a test for altered gating in the *Loa* mutant dynein, we measured its Michaelis

constant for ATP, K_{mATP}. Despite the somewhat decreased V_{max} for *Loa*$^{+/-}$-mouse dynein because of its higher K_{mMT} (Fig. 1c), the K_{mATP} was clearly decreased (18.8 ± 4.1 μM, compared with 27.0 ± 6.5 μM for wild-type, $P < 0.05$; Fig. 5c). This result is consistent with a defect in communication between motor domains, allowing premature ATP binding by the apo motor domain, and subsequent release from the microtubule (Fig. 5d). Further kinetic analysis will be needed to confirm this model.

These results have implications for intramolecular regulation of cytoplasmic dynein motor activity. Despite the location of the *Loa* mutation within the dynein tail, we find several lines of evidence for an altered interaction between dynein and microtubules, which is direct evidence for communication between the dynein motor and tail domains. The clear defect we observed in mutant dynein processivity raises the possibility of motor domain miscoordination. Supporting this, we identified novel defects in the *Loa*-mutant dynein: both an increase in lateral stepping on the microtubule lattice, and an increased affinity for ATP that apparently leads to premature run termination. Consistent with the subtly decreased stability of the *Loa*-mutant dynein complex, we propose that an abnormal linkage within the base of the *Loa*-mutant dynein molecule disrupts coordination between the two motor domains by altering their relative positioning and ability to interact laterally.

These results also suggest a role for processivity defects in disease causation. Neurodegeneration in the *Loa*$^{+/-}$ mutant mouse is unlikely to result from dynein subunit dissociation, as no dissociation was detected for the *Loa*$^{+/-}$ complex in cytosolic extracts or following purification (only dynein from the *Loa*$^{-/-}$ mouse, which dies shortly after birth, shows evidence of dissociation; Supplementary Information, Fig. S2). The data also argue against a loss in the association of dynein with membranous cargo, which persisted in our biochemical analysis. The most marked change observed to result from the *Loa* mutation was a decrease in dynein run-length. This effect quantitatively accounted for the observed defect in axonal transport, as indicated by a combination of empirical analysis with computational modelling. The neurons that are most likely to be affected by this defect in processivity and impairment in transport would be those with the longest axons, such as motor and sensory neurons. Our study therefore provides the first evidence that altered motor protein processivity can have pronounced consequences for *in vivo* transport, the impairment of which clearly correlates with neuronal death and disease.

METHODS

Methods and any associated references are available in the online version of the paper at http://www.nature.com/naturecellbiology/

Note: Supplementary Information is available on the Nature Cell Biology website

ACKNOWLEDGEMENTS

We thank R. McKenney for help with the quantum dot assays and useful discussion, and M. Vershinnin for developing the tracking program. This work was supported by NIH grants GM47434 (to R.B.V.), RO1GM070676 (to S.P.G.) and GM008798-09 (to K.M.O.M.), AHA grant 825278F (to J.X.), and the Columbia University Motor Neuron Center.

AUTHOR CONTRIBUTIONS

K.M.O.M., J.X., S.P.G. and R.B.V. designed the research. K.M.O.M. and J.X. performed experiments and analysed data. K.M.O.M., J.X., S.P.G. and R.B.V. wrote the paper.

COMPETING INTERESTS STATEMENT

The authors declare no competing financial interests.

Published online at http://www.nature.com/naturecellbiology
Reprints and permissions information is available online at http://npg.nature.com/reprintsandpermissions/

1. Paschal, B. M. & Vallee, R. B. Retrograde transport by the microtubule associated protein MAP 1C. *Nature* **330,** 181–183 (1987).
2. Hafezparast, M. *et al.* Mutations in dynein link motor neuron degeneration to defects in retrograde transport. *Science* **300,** 808–812 (2003).
3. Puls, I. *et al.* Mutant dynactin in motor neuron disease. *Nat. Genet.* **33,** 455–456 (2003).
4. Lai, C. *et al.* The G59S mutation in p150(glued) causes dysfunction of dynactin in mice. *J. Neurosci.* **27,** 13982–13990 (2007).
5. Chevalier-Larsen, E. S., Wallace, K. E., Pennise, C. R. & Holzbaur, E. L. Lysosomal proliferation and distal degeneration in motor neurons expressing the G59S mutation in the p150Glued subunit of dynactin. *Hum. Mol. Genet.* **17,** 1946–1955 (2008).
6. Kieran, D. *et al.* A mutation in dynein rescues axonal transport defects and extends the life span of ALS mice. *J. Cell Biol.* **169,** 561–567 (2005).
7. Myers, K. R. *et al.* Intermediate chain subunit as a probe for cytoplasmic dynein function: biochemical analyses and live-cell imaging in PC12 cells. *J. Neurosci. Res.* **85,** 2640–2647 (2007).
8. Chen, X. J. *et al.* Proprioceptive sensory neuropathy in mice with a mutation in the cytoplasmic Dynein heavy chain 1 gene. *J. Neurosci.* **27,** 14515–14524 (2007).
9. Ilieva, H. S. *et al.* Mutant dynein (*Loa*) triggers proprioceptive axon loss that extends survival only in the SOD1 ALS model with highest motor neuron death. *Proc. Natl Acad. Sci. USA* **105,** 12599–12604 (2008).
10. Perlson, E. *et al.* A switch in retrograde signaling from survival to stress in rapid-onset neurodegeneration. *J. Neurosci.* **29,** 9903–9917 (2009).
11. King, S. J., Bonilla, M., Rodgers, M. E. & Schroer, T. A. Subunit organization in cytoplasmic dynein subcomplexes. *Protein Sci.* **11,** 1239–1250 (2002).
12. Shpetner, H. S., Paschal, B. M. & Vallee, R. B. Characterization of the microtubule-activated ATPase of brain cytoplasmic dynein (MAP 1C). *J. Cell Biol.* **107,** 1001–1009 (1988).
13. Ross, J. L., Wallace, K., Shuman, H., Goldman, Y. E. & Holzbaur, E. L. Processive bidirectional motion of dynein–dynactin complexes *in vitro*. *Nat. Cell Biol.* **8,** 562–570 (2006).
14. Mallik, R., Carter, B. C., Lex, S. A., King, S. J. & Gross, S. P. Cytoplasmic dynein functions as a gear in response to load. *Nature* **427,** 649–652 (2004).
15. Reck-Peterson, S. L. *et al.* Single-molecule analysis of Dynein processivity and stepping behavior. *Cell* **126,** 335–348 (2006).
16. McKenney, R. J., Vershinin, M., Kunwar, A., Vallee, R. B. & Gross, S. P. LIS1 and NudE induce a persistent dynein force-producing state. *Cell* **141,** 304–314 (2010).
17. Mallik, R., Petrov, D., Lex, S. A., King, S. J. & Gross, S. P. Building complexity: an *in vitro* study of cytoplasmic dynein with *in vivo* implications. *Curr. Biol.* **15,** 2075–2085 (2005).
18. King, S. J. & Schroer, T. A. Dynactin increases the processivity of the cytoplasmic dynein motor. *Nat. Cell Biol.* **2,** 20–24 (2000).
19. Kardon, J. R., Reck-Peterson, S. L. & Vale, R. D. Regulation of the processivity and intracellular localization of *Saccharomyces cerevisiae* dynein by dynactin. *Proc. Natl Acad. Sci. USA* **106,** 5669–5674 (2009).
20. Zhang, Q. *et al.* Nudel promotes axonal lysosome clearance and endo-lysosome formation via dynein-mediated transport. *Traffic* **10,** 1337–1349 (2009).
21. Shubeita, G. T. *et al.* Consequences of motor copy number on the intracellular transport of kinesin-1-driven lipid droplets. *Cell* **135,** 1098–1107 (2008).
22. Hendricks, A. G. *et al.* Motor coordination via a tug-of-war mechanism drives bidirectional vesicle transport. *Curr. Biol.* **20,** 697–702 (2010).
23. Wang, Z., Khan, S. & Sheetz, M. P. Single cytoplasmic dynein molecule movements: characterization and comparison with kinesin. *Biophys. J.* **69,** 2011–2023 (1995).
24. Shima, T., Imamula, K., Kon, T., Ohkura, R. & Sutoh, K. Head–head coordination is required for the processive motion of cytoplasmic dynein, an AAA+ molecular motor. *J. Struct. Biol.* **156,** 182–189 (2006).
25. Sweeney, H. L. *et al.* How myosin VI coordinates its heads during processive movement. *EMBO J.* **26,** 2682–2692 (2007).
26. Gennerich, A. & Vale, R. D. Walking the walk: how kinesin and dynein coordinate their steps. *Curr. Opin. Cell Biol.* **21,** 59–67 (2009).

DOI: 10.1038/ncb2127

METHODS

Protein purification. Cytoplasmic dynein was purified from the brains of wild-type- and *Loa*$^{+/-}$-adult mice by microtubule-affinity, ATP release and sucrose density gradient fractionation, as previously described[1]. For purification of dynein from postnatal day zero (P0) brains, cytosol from three P0 brains was subjected to sucrose density gradient fractionation, microtubule-affinity in the presence of GTP (to remove kinesin), then ATP extraction to release dynein (Supplementary Information, Fig. S3c, d).

Sucrose density gradients. Whole-brain cytosol from P0 mice was fractionated on a 5–20% Tris-KCl sucrose gradient (20 mM Tris-HCl at pH 7.6, 50 mM KCl, 5 mM MgSO4 and 0.5 mM EDTA; ethylenediaminetetraacetic acid), or was incubated with 0.075 M, 0.15 M or 0.30 M potassium iodide (KI) on ice for 1 h, then fractionated on a sucrose gradient containing 0.075 M, 0.15 M, or 0.30 M KI. Fractions were analysed by SDS–PAGE (sodium dodecyl sulfate polyacrylamide gel electrophoresis) and western blotting using antibodies against dynein heavy chain[27] (1:1,000) and dynein intermediate chain (1:3,000; clone 74.1, K. Pfister, University of Virginia, USA). A solution of thyroglobulin, ferritin, catalase, lactate dehydrogenase and albumin was fractionated on a sucrose gradient to determine S values for the gradient fractions.

Biochemical assays. ATPase assays were performed using the malachite green method, as previously described[12], in Tris-KCl buffer containing 10 mM KCl or 50 mM KCl. Assays were incubated at 37 °C for 15 min in the presence of 1 mM ATP. For ATPase activity as a function of microtubules, taxol-stabilized microtubules (Cytoskeleton) were added to a solution containing 1 μg of dynein before adding ATP to start the reaction. For ATPase activity as a function of ATP, all reactions were performed in Tris-KCl buffer containing 10 mM KCl and in the presence of 10 μM microtubules. Activities were plotted at the range of microtubule or ATP concentrations. Michaelis-Menten curves were fit to the data to derive K_m and V_{max} values.

For microtubule-binding experiments, 1 μg of dynein was incubated with taxol-stabilized microtubules at a final concentration of 2.5 μM for 15 min at 37 °C, followed by centrifugation. Supernatant and microtubule pellet were either recovered for analysis, or the pellet was resuspended in Tris-KCl buffer containing 10 mM ATP, incubated at 37 °C for 15 min, and centrifuged. Supernatants and pellets were analysed by SDS–PAGE and western blotting using antibodies against dynein intermediate chain and tubulin (1:5,000; Sigma).

Membrane flotation analysis was performed as previously described[10]. Briefly, two P0 brains from each genotype were homogenized and centrifuged at 30,000*g*. The supernatant was centrifuged at 150,000*g*. The high-speed pellet was fractionated by flotation through a 2M, 1.5M and 0.6M sucrose step gradient. Membrane vesicles floated to the 0.6–1.5M interface. Samples were taken from the 0.6M layer, the vesicle interface, and the 1.5 M layer, for SDS–PAGE, and western blot analysis using antibodies against dynein intermediate chain and heavy chain, and synaptotagmin (1:500; StressGen) as a marker for vesicles.

Quantum dot assays. *In vitro* motility assays were conducted in flow chambers assembled from a glass slide and acid-washed cover slip, using double-sided adhesive tape (chamber volume, approximately 10 μl). Solutions were incubated in the chamber for 10 min. The chamber was incubated with 5 mg ml^{-1} biotin–BSA (bovine serum albumin), washed twice with 20 μl blocking buffer (30 mM HEPES at pH 7.2, 50 mM potassium acetate, 2 mM magnesium acetate, 1 mM EGTA (ethylene glycol tetraacetic acid), 10% (v/v) glycerol, 1 mg ml^{-1} BSA and 1 mg ml^{-1} casein), incubated with 5 mg ml^{-1} streptavidin solution, washed twice, then incubated with rhodamine- and biotin-labelled microtubules and washed twice again with blocking buffer containing 5 μM taxol.

Monoclonal anti-74.1 intermediate chain antibody (350 nM), polyclonal anti-heavy chain antibody (450 nM) or polyclonal anti-R1B2 antibody (450 nM), were mixed with goat anti-mouse or goat anti-rabbit quantum dots (350 nM; Invitrogen) in blocking buffer for 30 min on ice. Different antibodies gave similar results. Dynein (10 nM) was added to the antibody–quantum dot mixture and incubated on ice for 30 min. Similar results were obtained at 1:50 protein:quantum dot ratios. The dynein–quantum dot mixture was diluted 50 times immediately before chamber incubation, then washed twice. Blocking buffer containing 500 μM ATP, 5 μM taxol and an oxygen scavenging solution was flowed into the chamber. Differences in run-lengths and velocities between optical trap and quantum-dot assays were because of differences in ATP concentration. Single quantum-dot-labelled-dynein molecules were visualized at 25 °C on an inverted microscope (DMIRBE, Leica) using a Qdot 525 filter set (Omega Optical). Images were captured on a CCD (charged coupled device) camera (CoolSnap HQ, Photometrics) at 5 frames s^{-1}. The movement of individual dynein–quantum dots was analysed using a custom-tracking program (Gross Lab) to identify the quantum dot position versus time through two dimensional Gaussian fitting of their brightness profile. A processive run is defined here as motion > 200 nm that is terminated by detachment from the microtubule. A bidirectional run is a > 200 nm run in one direction, then a > 200 nm run in the opposite direction. In the case of a bidirectional run, the run-length was measured as the sum of processive run-lengths in both directions.

Optical-trapping experiments. Optical-trap assays, data recording, particle tracking and stalling-force analysis were performed as previously described[14,28–30]. Dynein was attached directly to polystyrene beads (PolySciences). Using antibody as a linker impaired the motility of the beads. The fraction of beads bound to microtubules was used to assess the average number of available motors per bead: 50–100% binding fractions correspond to the few motor condition, whereas ≤ 30% binding fractions correspond to the single-motor range[14,31,32]. Dynein-coated beads were positioned above a microtubule for 20–30 s using an optical trap. A binding event was scored on bead binding and evidence of processive motion. A sub-population of beads bound the microtubule, but did not demonstrate clear processive motion while in the trap (producing force <0.5pN). They moved bi-directionally along the microtubule once the trap was turned off at speeds independent of ATP concentration (1 versus 0.2mM ATP). These events were not biased toward mutant dynein. They were scored as binding, but were not used toward motility quantification owing to lack of normal force production. Motility and stalling force measurements were conducted using 500 nm polystyrene beads in assay buffer (10 mM PIPES, 2 mM MgSO4, 1 mM EGTA, 1 mM DTT (dithiothreitol), 50 mM potassium acetate and 10% (v/v) glycerol, at pH 6.9) supplemented with scavenging solution[33] and 1 mM ATP immediately before measurements. A custom-designed automated program monitored the bead position, then turned off the trap on detection of processive bead motion. An individual run was defined as the course between a bead binding to, and then detaching from a microtubule. For stall-force measurements, a trap stiffness of 2.2 pN per 100 nm was used. A stall was scored if the bead proceeded away from trap centre and held its plateau position for > 200 ms before detachment.

Step-size analysis was carried out on continuous segments of force traces where the systematic noise was no greater than approximately 8 nm, using an objective, model-independent, step-detection method[34], cross verified using a chi-square reduction method[35], and tested for kinesin stepping *in vitro*[36].

Lateral position experiments were conducted using 200 nm beads[23] in assay buffer with scavenging solution and 0.2 mM ATP. We examined the lateral movement of dynein by quantifying the change in a bead's lateral position between subsequent frames. Runs longer than 200 nm and 2 s were analysed. To limit possible bias toward longer travels, runs for each genotype were grouped into five different travel ranges (increments of 100 nm from 200 to > 600 nm). The final distribution of lateral changes describes the mean ± s.d. from averaging each subgroup.

Modelling of multiple motor conditions. We adapted a recently developed Monte Carlo model that closely reproduced force measurements for multiple dyneins *in vitro*[16], constrained by our experimental measurements of single-motor processivity for dyneins from wild-type, *Loa*$^{+/-}$, and *Loa*$^{-/-}$ mice. A 'run' is initiated when at least one of the N motors becomes stochastically bound to the microtubule (characterized by on-rate), and terminated when all N motors become detached (characterized by off-rate). For each motor, we used the same dynein stiffness (0.32 pN nm^{-1}), viscosity (10^{-3} N s^{-1} per m^2), on-rate estimation (1/s) and step size (8 nm), as well as formulas for stepping direction, velocity and off-rate under load, as described in ref. 16. The off-rate of dynein under no load was the lone adjusted parameter in our simulation, and was assumed to represent the sole differentiating factor between each genotype. To estimate the appropriate off-rate (under no load) for each genotype *in vivo*, we evaluated the average run-length *in vitro* when only one motor was available for transport. To account for potential *in vivo* factors, simulations were carried out that assumed a two-fold processivity enhancement of dynactin[18,19], and a 0.1 pN constant opposing force to account for viscous drag in cytosol.

Live-cell imaging of lysosomes. Hippocampal neurons were cultured from E19 mouse embryos, as previously described, and cultured for 4–6 DIV (days *in vitro*)[37]. Mice were cared for and treated according to IACUC regulations. For experiments, cultures were incubated in fresh media containing 500 μM lysotracker, washed, then imaged in 2 ml of fresh media (with 10 mM HEPES) at 37°C with 5% CO_2, on an Olympus IX81 inverted microscope. Images were captured at 5 frames s^{-1} for 1.5 min using an Hamamatsu ORCA-R2 CCD camera. Experiments were performed at least three times per genotype. For velocity, the motions of single lysosomes were analysed using kymographs generated with the 'Multiple Kymograph' plug-in for ImageJ (EMBL, Germany). For run-length, individual lysosomes were identified by a 2D Gaussian fitting of their brightness profile, and custom analysis routines identified periods of uninterrupted motion (runs), where net travel for any three consecutive frames (400 ms) was at least 80 nm in the minus-end direction.

Statistical methods. Distribution of run lengths was fitted to a first-order exponential decay. The fitted decay constant (and uncertainty) represents mean run length (and s.e.m.). Distribution of velocities was fitted to a Gaussian function. The fitted Gaussian peak position (and uncertainty) represents mean velocity (and s.e.m.). Distribution of stalling force was fitted to a Gaussian function. The fitted Gaussian peak position (and half width half maximum) represents the single-motor stall force (and s.d.). Statistical significance was determined using the Student's *t*-test.

27. Mikami, A., Paschal, B. M., Mazumdar, M. & Vallee, R. B. Molecular cloning of the retrograde transport motor cytoplasmic dynein (MAP 1C). *Neuron* **10,** 787–796 (1993).
28. Carter, B. C., Shubeita, G. T. & Gross, S. P. Tracking single particles: a user-friendly quantitative evaluation. *Phys. Biol.* **2,** 60–72 (2005).
29. Vershinin, M., Carter, B. C., Razafsky, D. S., King, S. J. & Gross, S. P. Multiple-motor based transport and its regulation by Tau. *Proc. Natl Acad. Sci. USA* **104,** 87–92 (2007).
30. Vershinin, M., Xu, J., Razafsky, D. S., King, S. J. & Gross, S. P. Tuning microtubule-based transport through filamentous MAPs: the problem of dynein. *Traffic* **9,** 882–892 (2008).
31. Svoboda, K., Schmidt, C. F., Schnapp, B. J. & Block, S. M. Direct observation of kinesin stepping by optical trapping interferometry. *Nature* **365,** 721–727 (1993).
32. Svoboda, K. & Block, S. M. Force and velocity measured for single kinesin molecules. *Cell* **77,** 773–784 (1994).
33. Block S. M., Asbury, C. L., Shaevitz, J. W., & Lang, M. J. Probing the kinesin reaction cycle with a 2D optical force clamp. *Proc. Natl. Acad. Sci. USA* **100,** 2351-2356 (2003).
34. Kalafut, B. & Visscher, K. An objective, model-independent method for detection of non-uniform steps in noisy signals. *Comput. Phys. Commun.* **179,** 716–723 (2008).
35. Kerssemakers, J. W. *et al.* Assembly dynamics of microtubules at molecular resolution. *Nature* **442,** 709–712 (2006).
36. Carter, B. C., Vershinin, M. & Gross, S. P. A comparison of step-detection methods: how well can you do? *Biophys. J.* **94,** 306–319 (2008).
37. Grabham, P. W., Bennecib, M., Seale, G. E., Goldberg, D. J. & Vallee, R. B. Cytoplasmic dynein and LIS1 are required for growth cone remodeling and fast neurite outgrowth. *J. Neurosci.* **27,** 5823–5832 (2007).

nature cell biology

DOI: 10.1038/ncb2127

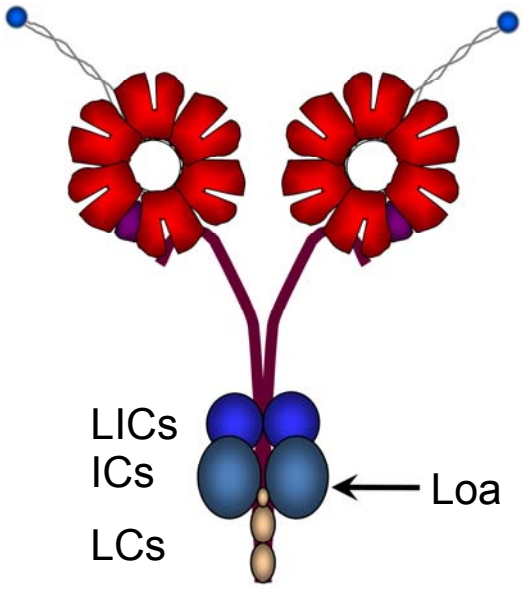

Figure S1 Cartoon depicting the position of the Legs at Odd Angles (Loa) mutation in the dynein heavy chain that is responsible for motor neuron disease and sensory neuropathy. The Loa mutation is at residue 580 within the HC-HC dimerization region and the IC binding region.

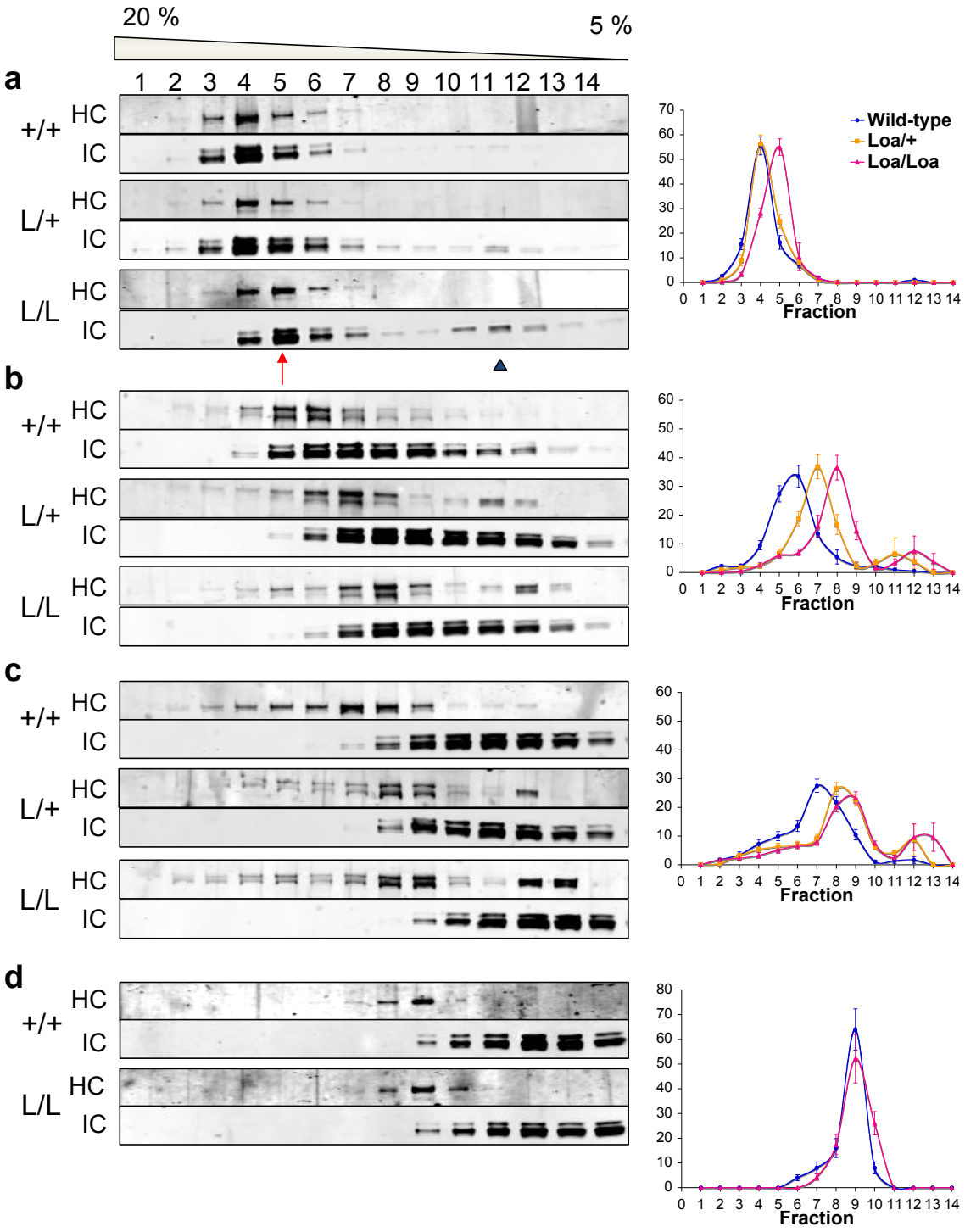

Figure S2 Effect of Loa mutation on cytoplasmic dynein complex stability. Mouse brain cytosolic extracts were fractionated by sucrose density gradient centrifugation and subjected to immunoblotting using dynein HC and IC antibodies. The HC sedimentation profiles were quantified, as shown at right. (**a**) Immunoblots of gradient fractions for wild-type (+/+), Loa/+, and Loa/Loa mouse brain lysates. Arrowhead indicates 6S peak position for dissociated ICs. A small, but clear shift in the peak position for the cytoplasmic dynein complex (arrow) is observed in the Loa/Loa dynein profile. **(b)** Sucrose gradients of brain lysate from wild-type and mutant mice with added KI (0.075M). The peak position for the dynein complex is shifted to lower s-values in each case, progressively so for Loa/+ and Loa/Loa mutant mice. Further dissociation of the dynein complex is observed at 0.15M (**c**) and 0.30M (**d**) KI.

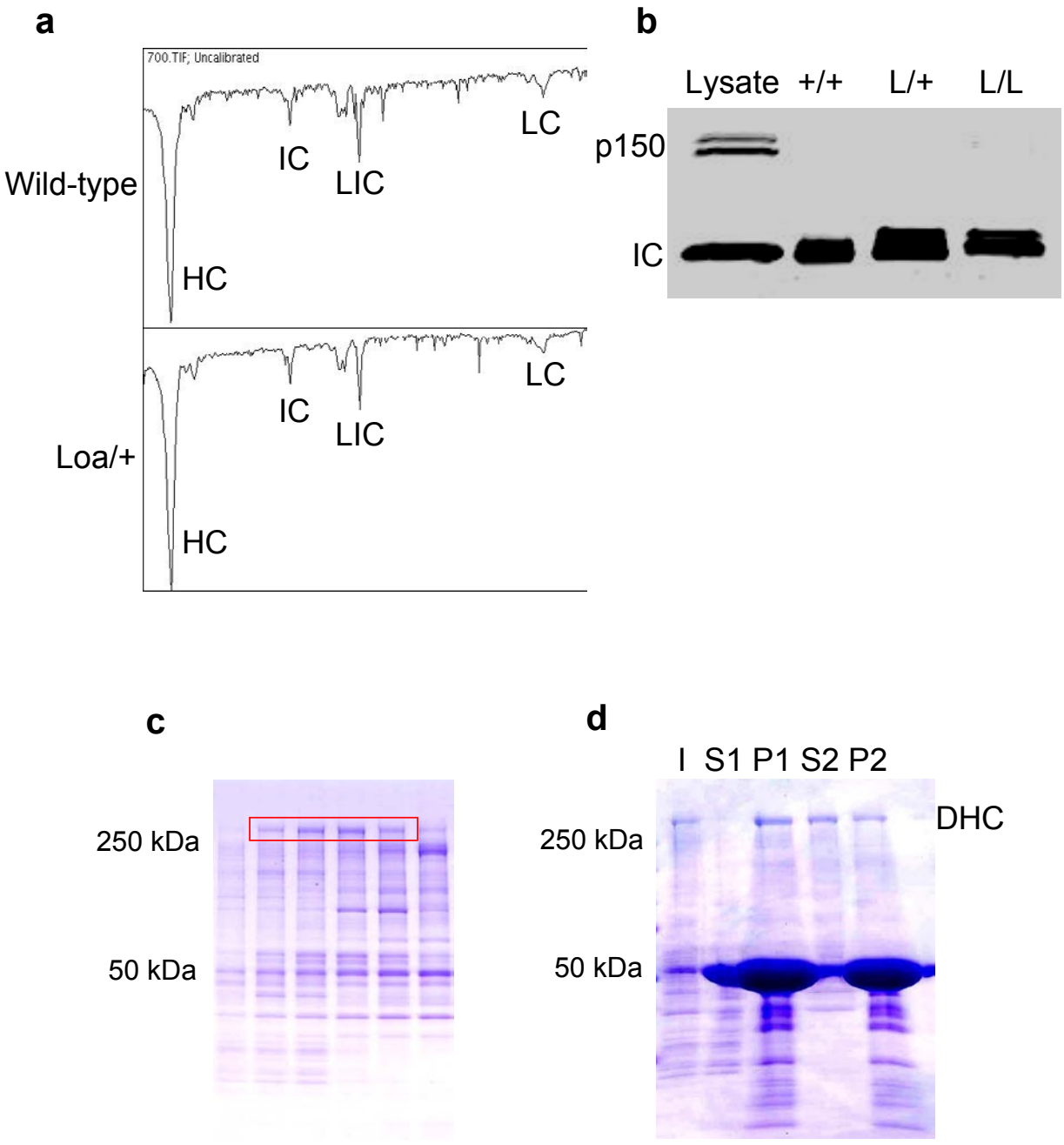

Figure S3 Wild-type and Loa mutant dynein preparations show similar subunit composition and lack dynactin. **(a)** Line graph depicting the band intensity for each subunit of the wild-type and Loa/+ dynein complex. This graph corresponds to the coomassie stained gel in Fig. 1B, and shows a similar composition between the wild-type and Loa/+ dynein, including a lack of dynactin. **(b)** Immunoblot of the p150 subunit of dynactin and the IC subunit of dynein in whole brain lysate (lane 1), and wild-type (lane 2), Loa/+ (lane 3), and Loa/Loa (lane 4) dynein. **(c-d)** Purification of Loa/Loa dynein from newborn pup brains. **(c)** Coomassie stained gel of sucrose density gradient fractions of mouse brain lysate. The fractions containing dynein HC are boxed in red. The dynein in these fractions was purified by microtubule affinity and ATP extraction as shown in **(d)**. The input (I) is 30 % of the total protein. Dynein is depleted from the supernatant (S1) and pellets with microtubules (P1) in the absence of ATP. In the presence of 10 mM ATP, dynein is released into the supernatant (S2) from the microtubule pellet (P2).

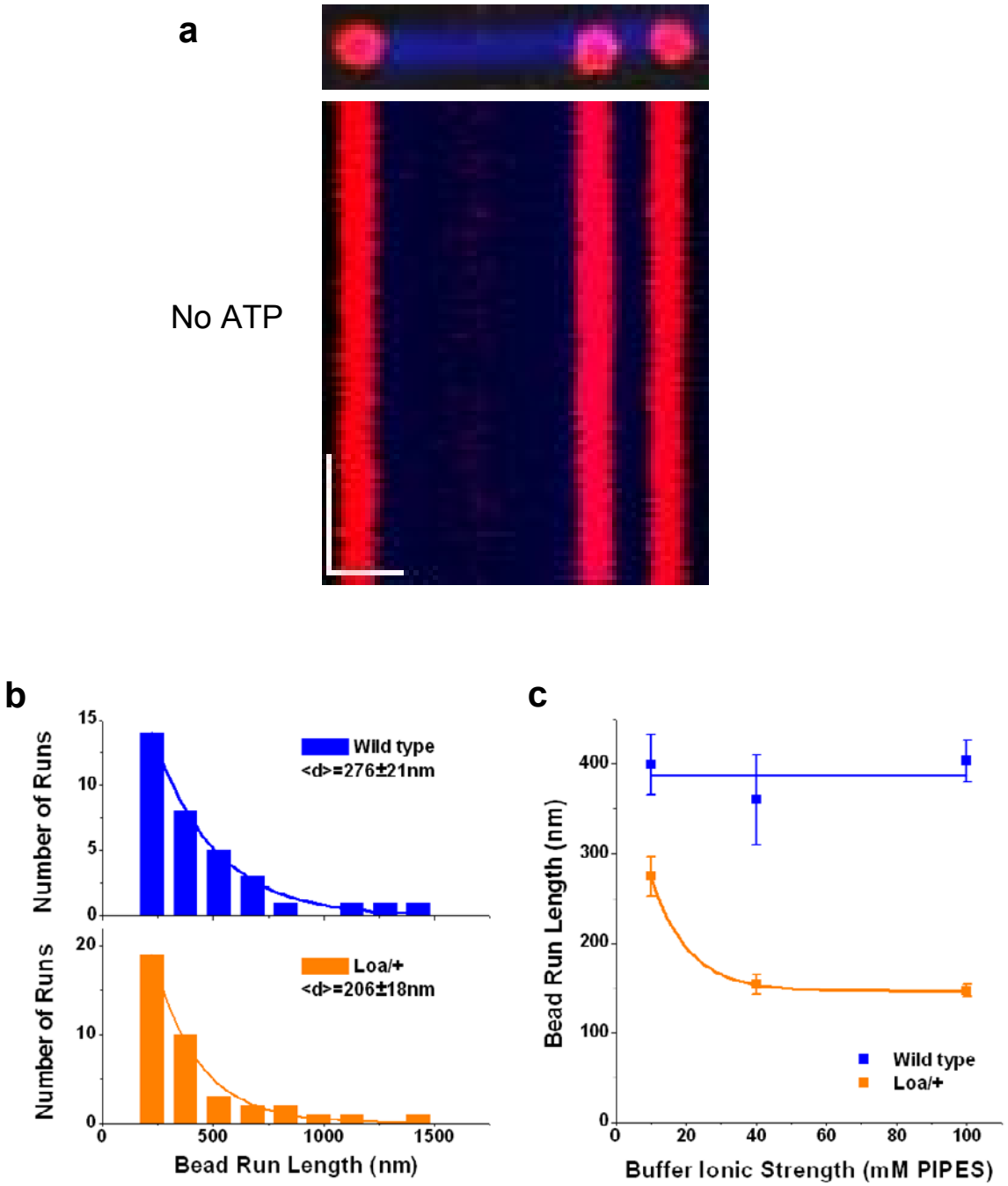

Figure S4 Biophysical analysis of dynein run-length using quantum dot and bead assays. **(a)** Representative kymograph of dynein attached quantum dots along a microtubule in the absence of ATP. Scale bars = 1 um (x-axis) and 5 sec (y-axis). (**b**) Distributions of bead run-length driven by a single Loa/+, or wild-type dynein (n > 34). (**c**) Increases in buffer ionic strength has no effect on bead run-length when carried by wild-type dynein, but suppresses Loa/+ runs down to ~40 % of wild-type travel. Comparisons were carried out at 75 % bead binding fraction. Average run-length at binding fractions below 70 % for Loa/+ dynein is shorter than our measurement limit for PIPES concentration ≥40 mM.

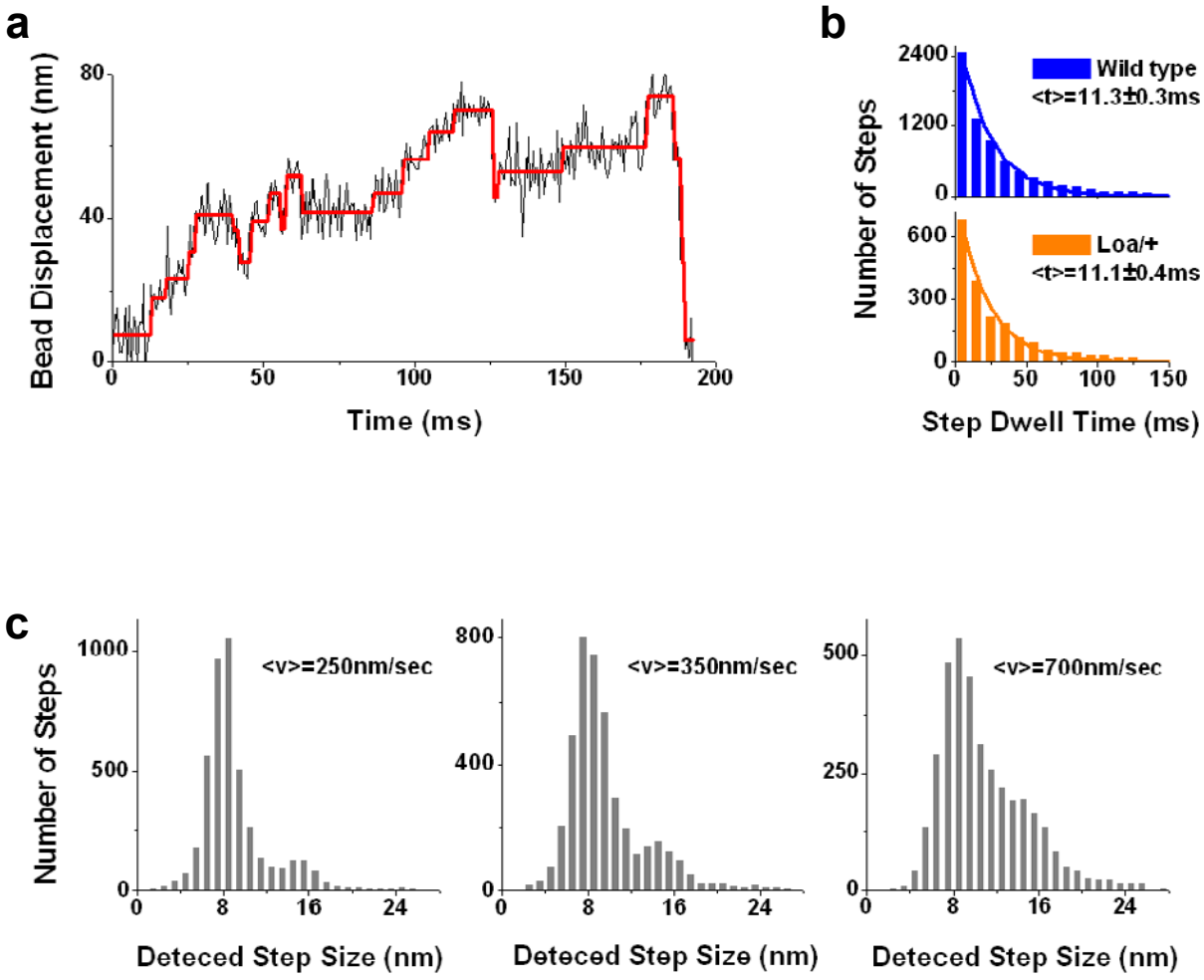

Figure S5 Effect of dynein velocity on step detection. **(a)** Sample trace for step detection of wild-type dynein under load (2.2 pN/100 nm stiffness, 1 mM ATP, sampled at 2 kHz) using Visscher algorithm. **(b)** The measured average step dwell time is ~11 ms for both wild-type and Loa/+ dynein (n > 1979), corresponding to an average off-rate of ~45 /sec for an individual dynein head. **(c)** Simulated data was generated using 8 nm step size with experimentally determined 6 nm Gaussian noise, and three distinct velocities, the fastest of which is the experimentally determined ~700 nm/sec. Each analysis set (n = 5000) reveals primarily 8 nm steps; however, there is an increasingly prominent 16 nm peak associated with higher velocity.

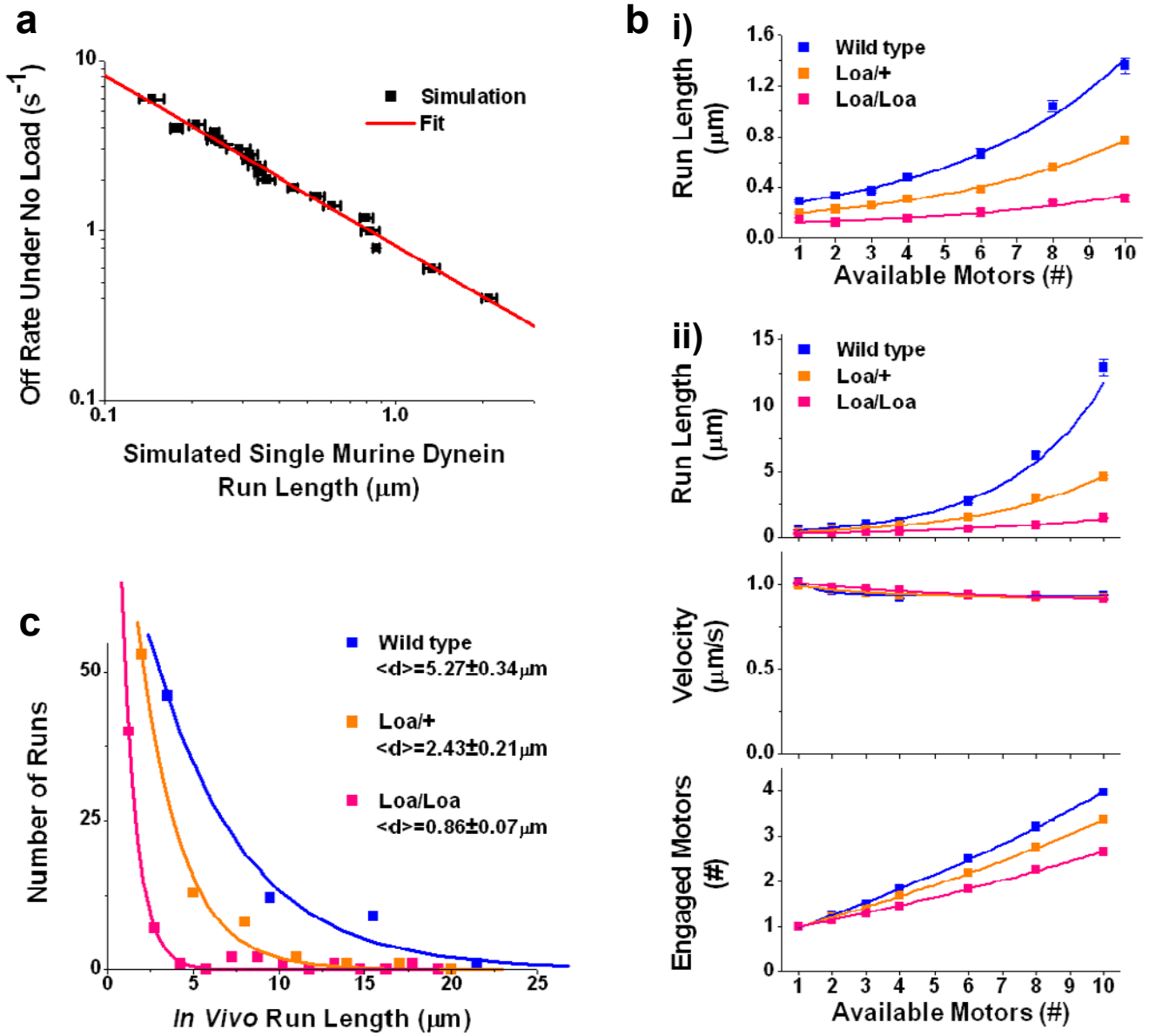

Figure S6 Theoretical study of multiple dynein transport using the measured *in vitro* processivities as the only differentiating factor between wild-type and mutant dyneins, and measurements of retrograde, lysosomal run-lengths in living neurons. **(a)** We simulated single dynein run-lengths for a range of dynein off-rates under no load (the only free parameter in our model, plotted points are mean ± SEM, n > 500 simulations). The resulting processivity *vs.* off-rate (under no load) curve is well described by a single exponential decay. **(b)** Based on the simulation results in **(a)**, we chose off-rates to match the experimentally measured single-molecule *in vitro* processivities for each genotype, and modeled their expected multiple-motor transport both in the absence of **(i)**, and presence of potential processivity factors present *in vivo*: dynactin, and viscous drag **(ii)**. The predicted average run-lengths demonstrate amplified processivity defects in the mutants when multiple dyneins are available for transport (**i**, **ii** top). Predicted instantaneous cargo velocity (**ii**, middle) is not significantly affected with increasing available motor numbers, nor is it altered by Loa mutation. However, the number of instantaneously engaged motors (**ii**, bottom) is reduced with decreasing processivity, thus leading to further reduction in the predicted multimotor run-lengths for Loa mutants. **(c)** Distributions of actual lysosomal travel through axons back towards the cell body in wild-type, Loa/+ and Loa/Loa neurons (n > 103, P<0.006).

Figure 1a

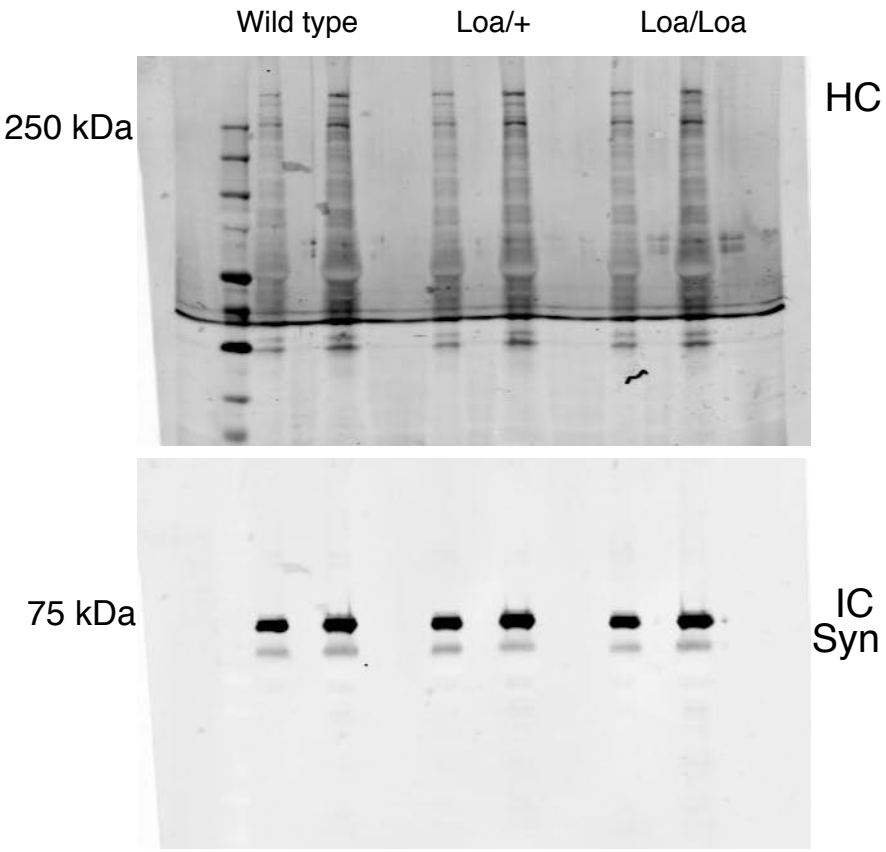

Figure S7 Uncropped data

Figure 1b

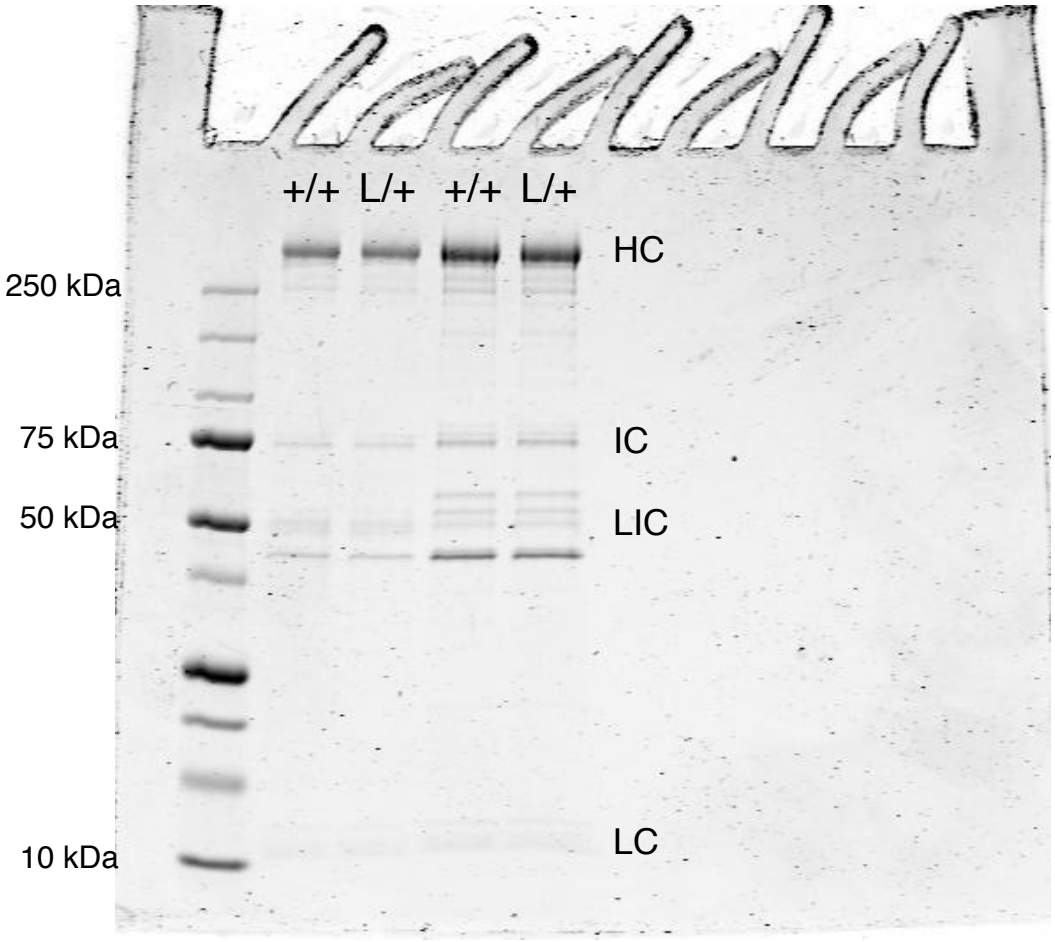

Figure S7 continued

Figure 1d

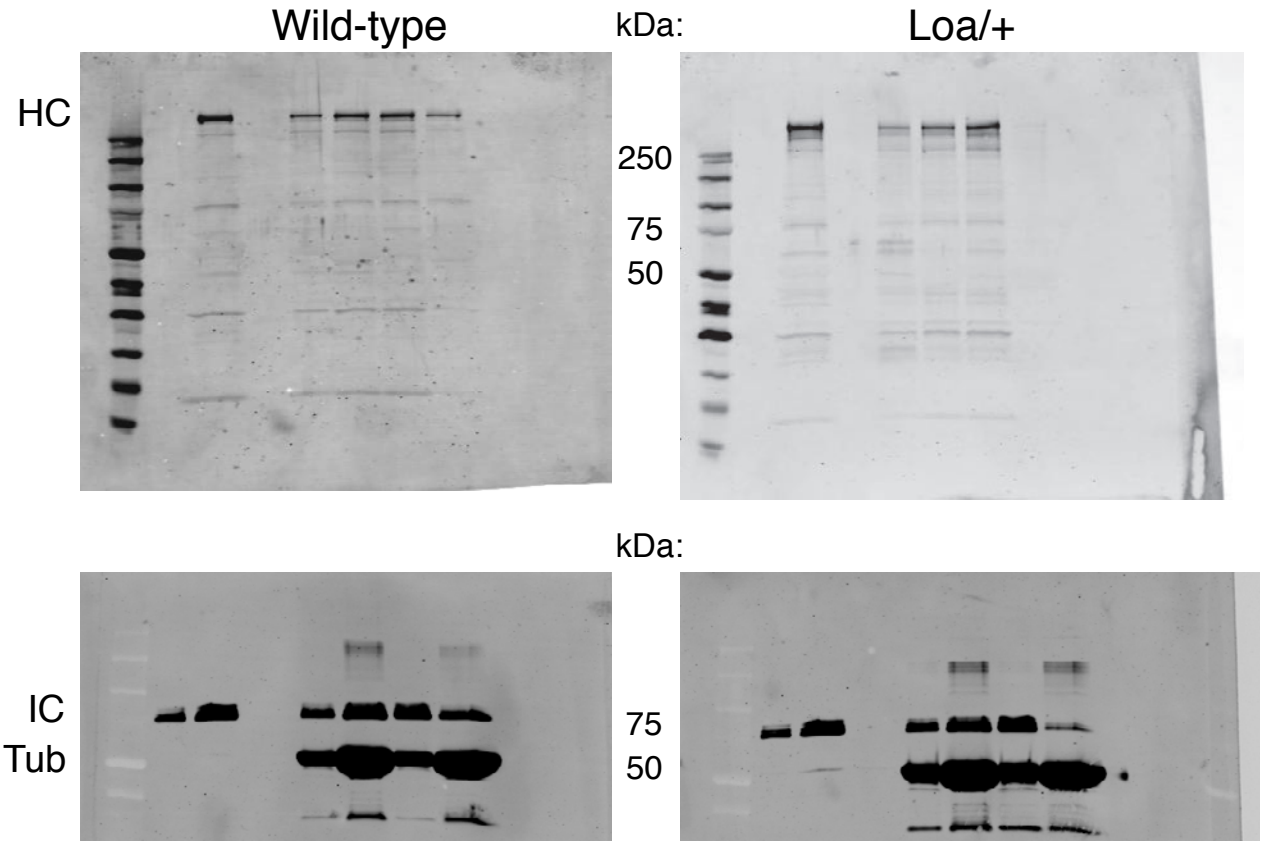

Figure S7 continued

Figure S2

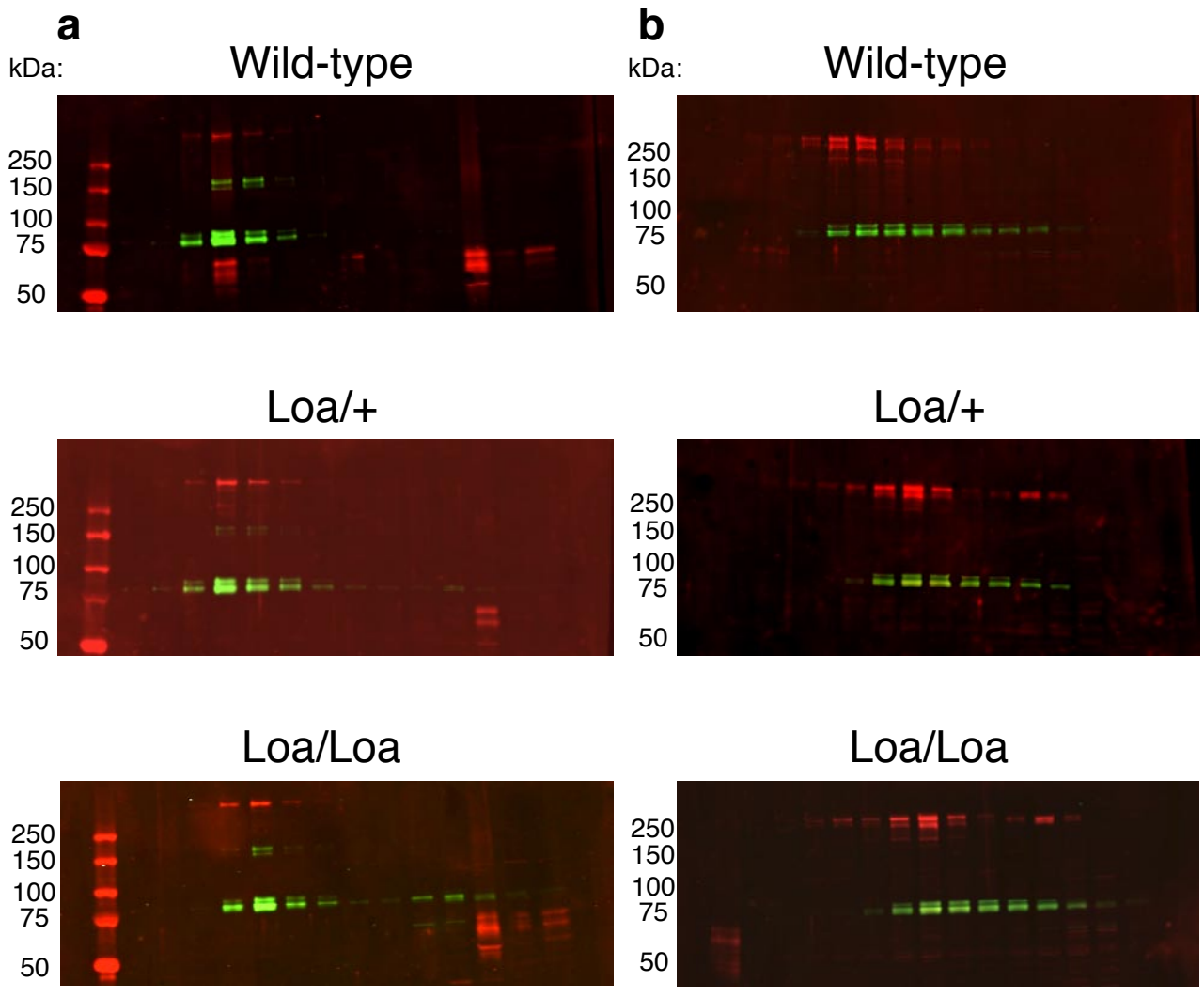

Red = HC
Green = IC

Figure S7 continued

Figure S2

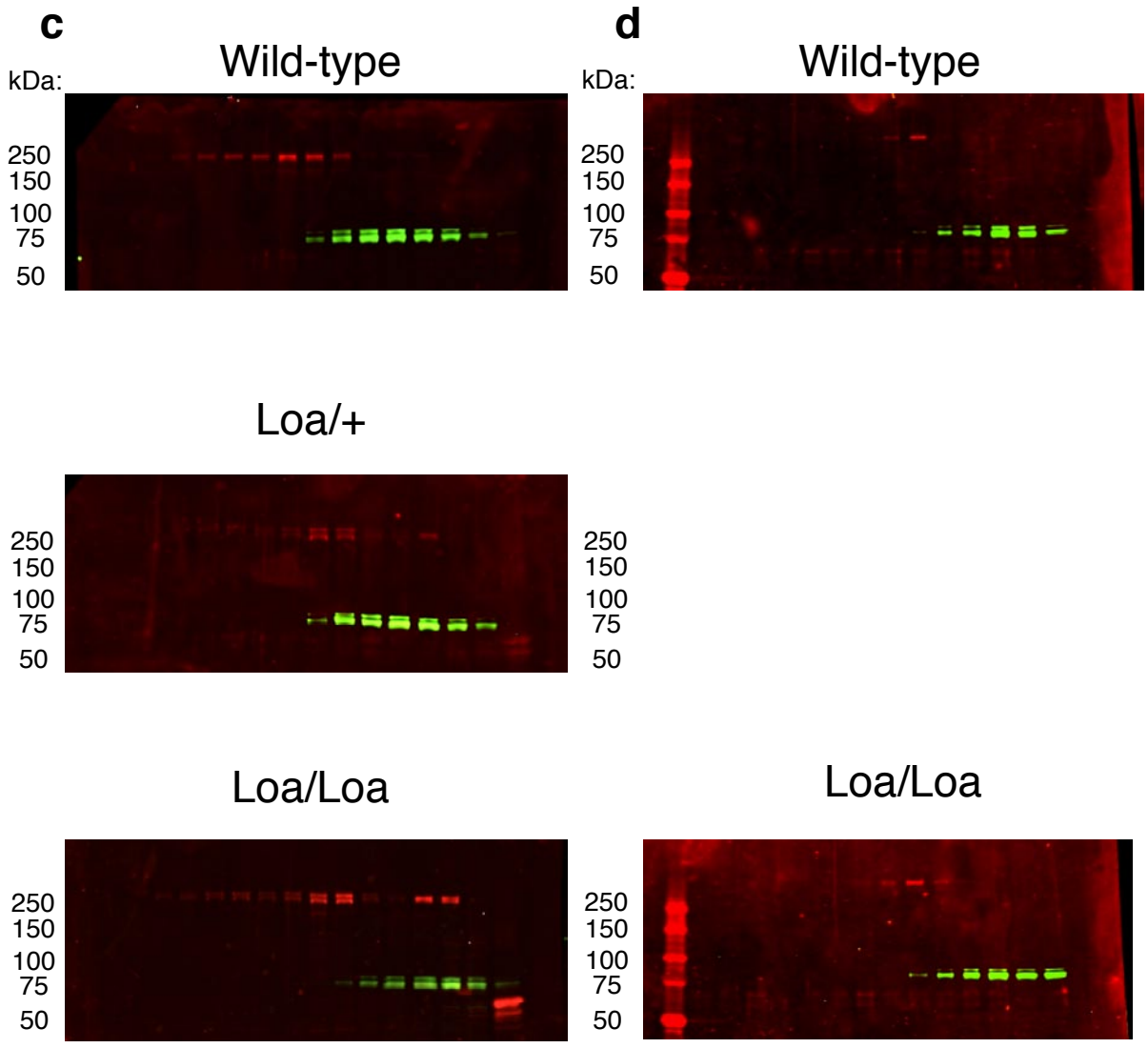

Figure S7 continued

Figure S3b

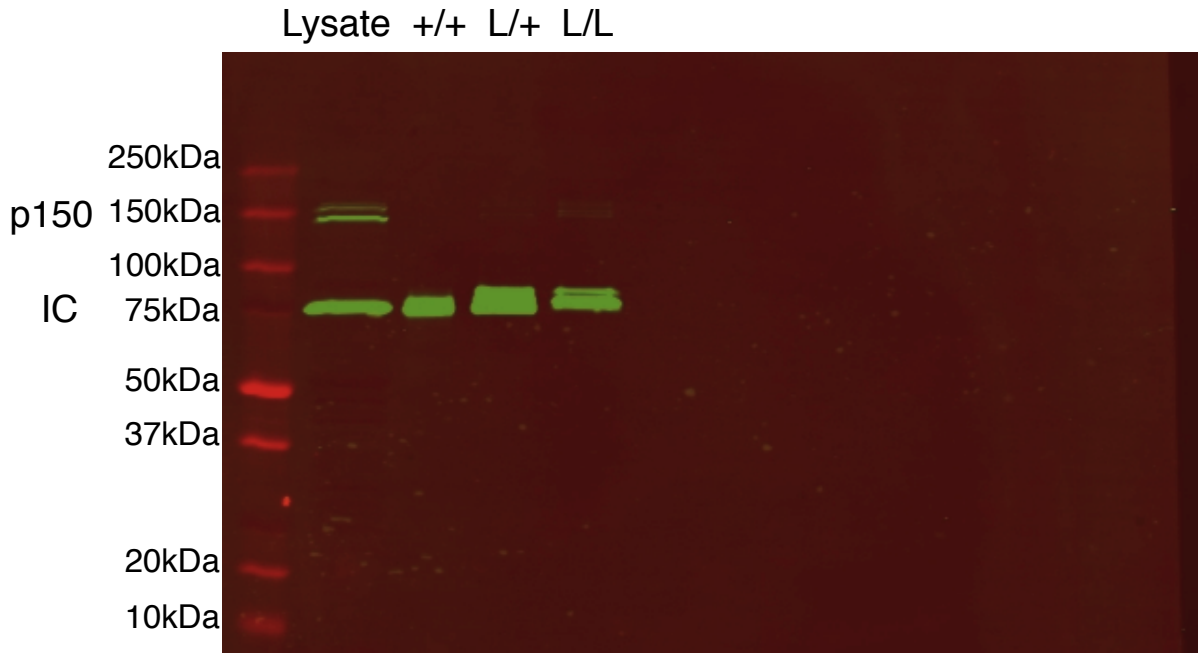

Figure S7 continued

Figure S3c-d

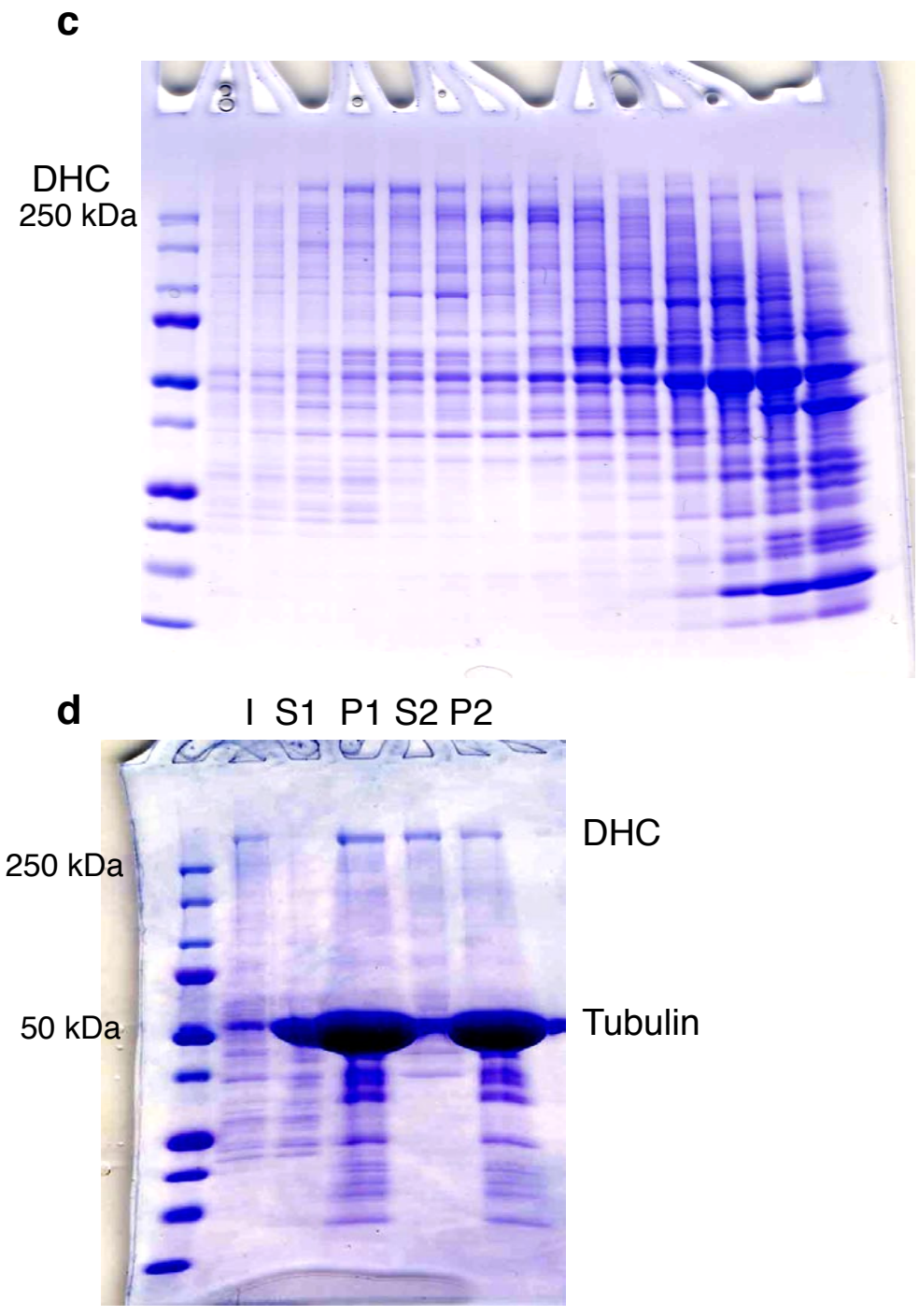

Figure S7 continued

SUPPLEMENTAL INFORMATION

Reversible dissociation of the dynein complex as revealed by sucrose gradient centrifugation analysis.

Potassium iodide (KI) is a chaotropic salt known to dissociate cytoplasmic dynein into two subcomplexes: one consisting of the HCs and LICs (light intermediate chains), and the other of the ICs and LCs (light chains)[1]. When brain cytosol was treated with increasing levels of KI, the low molecular weight IC peak gradually increased in size, whereas the HC exhibited a gradual decrease in s-value from ~20S to 9S, suggesting a reversible equilibrium between dimeric and monomeric HC polypeptides (Fig. S2)[2]. Thus, the intermediate s-values of the HC reflect its reversible self-association.

Loa mutation alters the off-rate of dynein molecules in the presence of ATP.

Processivity describes the average distance a single motor can travel along a microtubule before detachment. The ratio of processivity to velocity gives rise to the average association time between the motor and microtubule, while the ratio of velocity to processivity gives rise to the average detachment rate of the motor from the microtubule. Using the measured single-motor motilities under no load (Fig. 2, 3a, S4b), we calculated the off-rate of a dynein molecule to be 2.2 ± 0.2/sec for wild-type, 2.9 ± 0.1/sec for Loa/+, and 4.2 ± 0.2/sec for Loa/Loa in the presence of 500 μM ATP. In the presence of 1mM ATP, the off-rate would be an average of 3.0 ± 0.2/sec for wild-type, and 4.1 ± 0.4/sec for Loa/+ dynein. The experimentally determined off-rates under no load are in good agreement with those calculated from single motor processivities in our theoretical model under saturating ATP (Fig. S6a): 2.9/sec for wild-type dynein, and 3.97/sec for Loa/+, and 5.92/sec for Loa/Loa.

Bulk of larger axial steps detected arises from unresolved 8nm steps.

The majority of force traces used for step-size detection correspond to the motor moving away from the trap center at ~700-800 nm/s before stalling or falling back into trap center. To gain intuition on the effect of motor velocity on step detection, we generated simulated data sets assuming 8 nm step size, 6 nm Gaussian noise (~6-8 nm measured), and three distinct velocities (corresponding to 727 nm/s, 364 nm/s, and 242 nm/s), and carried out the exact same Visscher step-detection analysis[3]. We observed an increased prominence of a 16nm peak in the detected step size distribution with increasing velocity (Fig. S5), suggesting that the larger steps in Fig. S5 are artifacts of successive 8 nm steps not being resolved at the higher stepping rate. We found that this effect of combined steps at ~700 nm/sec was sufficient to account for the apparent increase in the 16nm peak in our experimentally measured step size distributions (Fig. 3c) from that found in yeast dynein[4].

Reduction in single motor processivity leads to reduced average cargo velocity in multiple motor transport.

For a cargo with a characteristic run-length d, at an instantaneous velocity v, and pausing duration p between detachment and re-attachment, the total distance D that the cargo can cover during the time interval T, is

$$D = \left[\frac{T}{\frac{d}{v}+p}\right]\bullet d + \left(T - \left[\frac{T}{\frac{d}{v}+p}\right]\bullet\left(\frac{d}{v}+p\right)\right)\bullet v = T\bullet v - \left[\frac{T}{\frac{d}{v}+p}\right]\bullet p\bullet v\,,$$

and the average velocity including pauses, V, is

$$V = \frac{D}{T} = v - \left[\frac{T}{\frac{d}{v} + p} \right] \bullet \frac{p \bullet v}{T},$$

where [X] is the greatest integer value less or equal to X.

We assumed that cargoes are transported by dynein only, and the only difference between genotypes is their respective single motor processivity. Using an average pausing duration of 0.6 second before a detached cargo re-binds to the microtubule for all three genotypes, and simulated run-lengths and velocities constrained by 7.7 dyneins per cargo (Fig. 4b), we find that the average cargo velocity over the course of 60 sec was reduced by 11% in Loa/+ and 37% in Loa/Loa from wild-type neurons.

References

1 King, S. J., Bonilla, M., Rodgers, M. E. & Schroer, T. A. Subunit organization in cytoplasmic dynein subcomplexes. *Protein Sci* **11**, 1239-1250. (2002).

2 Gilbert, G.A., & Jenkins, R. C. L. L. Boundary Problems in the Sedimentation and Electrophoresis of Complex Systems in Rapid Reversible Equilibrium. *Nature* **177**, 853-854 (1956).

3 Kalafut, B. & Visscher, K. An objective, model-independent method for detection of non-uniform steps in noisy signals. *Computer Physics Communications* **179**, 716-723 (2008).

4 Reck-Peterson, S. L. *et al*. Single-molecule analysis of Dynein processivity and stepping behavior. *Cell* **126**, 335-348 (2006).